Transportation Research Part C 128 (2021) 103220

Contents lists available at ScienceDirect

Transportation Research Part C

journal homepage: www.elsevier.com/locate/trc

Optimizing the integrated off-ramp signal control to prevent queue spillback to the freeway mainline

Yen-Yu Chen *, Yen-Hsiang Chen, Gang-Len Chang

Department of Civil and Environmental Engineering, University of Maryland, College Park, MD 20742, USA

ARTICLE INFO

Keywords:
Off-ramp area
Queue spillover
Signal control
Weaving maneuver
Mandatory lane change
Discretionary lane change

ABSTRACT

This study presents an integrated off-ramp control model that incorporates the impact of ramp queue spillback on the freeway mainline in design of the off-ramp intersection's signal plan. The proposed model consists of a mesoscopic traffic module to capture the complex interrelations between the freeway mainline's traffic state and the lane-changing maneuvers triggered by off-ramp queue spillback, and a local signal optimization module to maximize the total benefit for both the freeway and intersection in the vicinity of an interchange. Using the simulation–optimization solution logic, the proposed model will first estimate the off-ramp queue length, produced from the signal module, to assess the resulting impacts on the freeway mainline, and then feed such impacts back to the control objective to iteratively search for the optimal cycle length and phase durations with the genetic algorithm. To assess the effectiveness of the proposed model, this study has conducted a two-stage evaluation, where the first stage uses the extensive field data to confirm the reliability of its freeway queue impact module and the second stage focuses on evaluating the benefits of accounting for the queue impacts on the freeway in design of the off-ramp signal plan under various traffic scenarios. The results from extensive tests have confirmed that the proposed model can effectively minimize the likelihood of causing off-ramp queues to spill back to the freeway mainline, and the failing to incorporate such impacts in design of the off-ramp signal will contribute significantly to the formation of freeway bottlenecks in the interchange area.

1. Introduction

As is well recognized, weaving maneuvers by on-ramp vehicles and exiting off-ramp flows are two primary contributors to the formation of local freeway bottlenecks, because both may result in substantial speed reduction and excessive congestion in the vicinity of an interchange due to extensive mandatory and discretionary lane changes. Over the past several decades, a large body of ramp metering studies, ranging from pre-timed to real-time adaptive controls, has been proposed in the freeway control literature to address the impacts of high on-ramp flows and the resulting merges on the target freeway segments' traffic conditions. In contrast, the equally critical off-ramp control issue has not received the comparable attention by the traffic community, likely because off-ramp signals in most states are operated by local traffic agencies. As such, an off-ramp signal's vital role in balancing the congestion level between the freeway and arterials in the vicinity of an interchange has mostly been neglected, and its signal design is based typically on the volume distributions over all intersection approaches, supplemented with the progression offsets to facilitate the arterial's through-traffic

* Corresponding author.
E-mail addresses: yychen804@gmail.com (Y.-Y. Chen), yenchen@umd.edu (Y.-H. Chen), gang@umd.edu (G.-L. Chang).

https://doi.org/10.1016/j.trc.2021.103220
Received 4 June 2020; Received in revised form 19 March 2021; Accepted 9 May 2021
Available online 21 May 2021

flows.

In fact, for a signalized intersection receiving heavy volume from a freeway off-ramp, failing to account for the impacts of off-ramp queue spillback issue in design of its signal plan often yields insufficient green duration to discharge the off-ramp flows, and may even trigger the queues to spill back onto the freeway's rightmost lane during the peak hours. Such queue spillovers often result in not only a reduction in mainline throughput but also a potential breakdown. Some field studies from German (Kerner and Rehborn, 1997; Daganzo et al., 1999; Newell, 1999) and Oakland, CA (Muñoz and Daganzo, 2002) evidenced that off-ramp queues due to high exiting flows can propagate to the upstream freeway segments at quite fast speed, and result in significant delays or even partial lane-blockage. Cassidy et al. (2002) investigated the videotaped data from an off-ramp area to confirm that the distributions of queue spillovers are negatively correlated with the freeway mainline's discharging flow rates.

Among very few studies on the off-ramp related issues, Highway Capacity Manual (HCM) 6th edition (or HCM 2016) provides a set of analytical formulas to estimate the throughput with known off-ramp and through flow rates for planning applications. Daganzo (1997) constructed a continuum model that can be applied in practice to differentiate through and exiting streams on a freeway. Daganzo et al. (1999) and Muñoz and Daganzo (2002) further provided a mechanism to explain the jam on the freeway mainstream caused by exiting queues. Newell (1999) argued that such delay can also be approximated with a graphical solution. Spiliopoulou et al. (2014) evaluated the performance of two macroscopic traffic models, Cell Transmission Model (CTM) and METANET, at congested freeway off-ramp areas with the field data from a Greek motorway. The results showed that both models are able to reproduce traffic congestion due to an over-spilling off-ramp with sufficient accuracy.

Recognizing the capacity reduction and excessive delay caused by off-ramp spillovers, Li et al. (2009) proposed an off-ramp signal model to minimize the queue spillback from an off-ramp to the freeway mainline using the CTM to capture the traffic propagation both on freeway and surface streets. Lim et al. (2011) developed a sequential control model to minimize the total delay on the off-ramp and the connected downstream arterial segments. Zhao and Liu (2016) designed the optimal lane configuration and signal settings to maximize the off-ramp intersection's capacity, given the weaving and interactions between flows at the off-ramp and on the parallel surface street. Yang et al. (2014) proposed a two-stage control model that can optimize the signal plans on an arterial connected to an off-ramp and prevent its off-ramp queue from spilling onto the freeway mainline. An enhancement of such an algorithm for use under the adaptive control environment was provided later by Yang et al. (2018). Spiliopoulou et al. (2016) in their real-time freeway control model proposed a strategy for ensuring no off-ramp queue spillback to the freeway by imposing the ramp-flush function to discharge off-ramp queues to the receiving intersection.

To contend with the same off-ramp congestion issue, some studies (e.g., Liu et al., 2011; Spiliopoulou et al., 2013; Spiliopoulou et al., 2014; Spiliopoulou et al., 2018) in the literature proposed to adopt the route diversion plan to mitigate the recurrent freeway traffic congestion due to a saturated off-ramp. Conceivably, reducing the target ramp's volume by guiding drivers to an alternative off-ramp is a viable demand-side strategy. However, exercising effectively interactions with target drivers in real time so as to dynamically adjust the messages of guidance based on the compliance rate is a vital but quite complex task in practice. Moreover, traffic flows via either the target congested ramp or the alternate one under such a detour operation are subjected to the off-ramp signal control, and remain in need of an innovative off-ramp signal design as proposed in this study to facilitate the progression of the off-ramp flows over the arterial.

In view of the significant impacts of lane-changing intensity on a freeway's capacity, several lane-changing models from the microscopic perspective have been proposed to describe the lane-choice behaviors of freeway drivers (Gipps, 1986; Wiedemann and Reiter, 1992; Yang and Koutsopoulos, 1996; Toledo et al., 2007). Due to the inevitably large number of embedded parameters, such models are mostly used in traffic simulation software, but not for system-wide control applications. As such, some researchers over the past decades, for either traffic analysis needs or developing control systems, have explored the relationships between the lane-changing frequency and macroscopic traffic characteristics including lane density differences (Gazis et al., 1962; Oliver and Lam, 1965; Munjal and Pipes, 1971; Jin, 2010) and lane speed discrepancies (Laval and Daganzo, 2006). For example, Chang and Kao (1991) proposed a model to estimate the percentage of vehicles changing lanes on a freeway segment, based on the macroscopic traffic flow properties, including lane speeds, densities, flow rates, their ratios between lanes, average headway, and the headway variance.

Despite the progress made by traffic researchers on the off-ramp issues, the weaving impacts caused by queue spillovers on the freeway traffic dynamics are, however, not sufficiently addressed in most existing studies. Notably, the impact of an off-ramp spillover on the freeway's rightmost lane will inevitably intensify lane-changing behaviors and ultimately cause congestion. Specifically, the mandatory lane-changing (MLC) maneuvers by the exiting-to-off-ramp vehicles on a congested freeway segment will cause uneven speed distribution across all travel lanes, and consequently trigger extensive discretionary lane changes (DLC) by mainline vehicles to avoid speed reduction.

In brief, a freeway segment's traffic condition is likely to evolve to a near chaotic state and propagate the congestion to its upstream segments, if concurrently plagued by both types of extensive lane-changing maneuvers and capacity reduction due to a partial lane blockage by the off-ramp overflows. Hence, it is imperative that an off-ramp signal be designed with the control objective to prevent the off-ramp queue spillback and then maximize the total benefit for both the intersection and freeway segments in the interchange area. The primary objective of this study is to develop a signal control model, specially designed for those intersections directly receiving the off-ramp flows from a freeway mainline and responsible for not only minimizing the delay of its accommodated arterial flows, but also for preventing the formation of off-ramp queues to spill over to the freeway.

The rest of the paper is organized as follows. Next section presents the proposed off-ramp queue impact (OQI) module, including its lane-changing functions and the evaluation results from real-world data. This is followed by a detailed description of the integrated off-ramp signal control (IOSC) model and its validation results in Section 3. Concluding findings and future extensions are highlighted in the last section.

2. Off-ramp queue impact (OQI) module

This study attempts to contend with the issue of the off-ramp queue spillback, because it often results in not only a reduction in the freeway mainline's throughput and speed but also a partial lane blockage due mostly to the insufficient green duration allocated to the off-ramp flows at the off-ramp intersection. To optimize the performance of arterials and freeway mainline suffering from off-ramp queue spillover impacts, this study, as shown in Fig. 1, presents an IOSC model, consisting of the newly proposed Off-ramp Queue Impact (OQI) module and the intersection signal design module from the previous study (Chen and Chang, 2013). These two modules, interacting in a macroscopic simulation–optimization environment, will exert the iterative search of the optimal set of decision variables based on the pre-specified control objective.

The primary search process of the IOSC model includes the following steps:

- For the current time interval, the proposed OQI module will first calculate the ***exiting flow rate*** from the freeway mainline to the off-ramp, which is viewed as one approach's traffic volume to the off-ramp intersection.

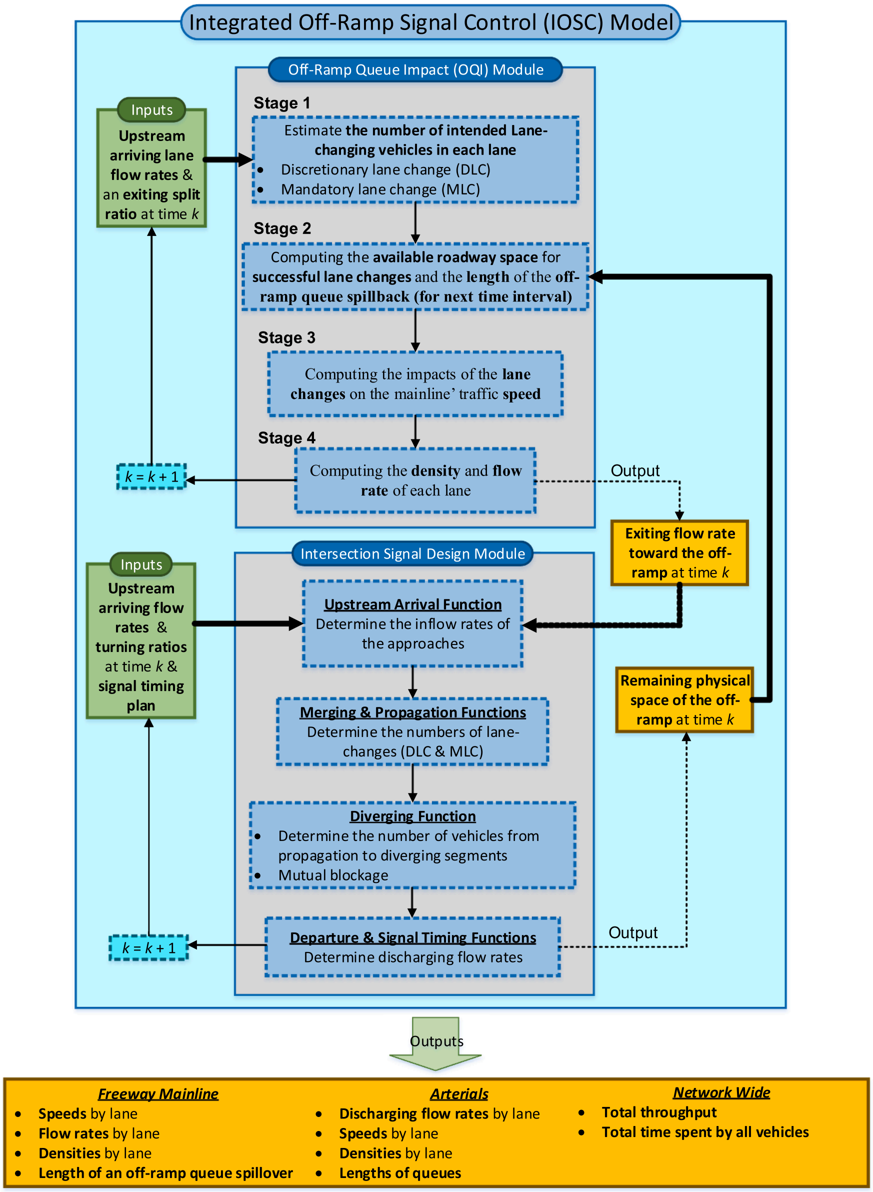

Fig. 1. Principal model components and operational flowchart of the IOSC model.

- At the same time interval, the intersection signal design module will compute the ***remaining physical space*** of the off-ramp for queue storage, based on the signal timing plan and flow evolution along the off-ramp.
- Based on the ***ramp exiting flow rate*** and the ***remaining physical space*** of the off-ramp, the OQI module will estimate the length of the queue spillover for the next time interval.
- Given the length of the queue spillover, the OQI module will then estimate its impacts on the freeway mainline's traffic conditions, including speeds, densities, mainline flow rates, and ***exiting flow rate*** to the off-ramp, at the same time interval.

2.1. Stages and formulations in the OQI module

Traffic flows on a freeway segment that are impeded by off-ramp queues generally exhibit a high frequency of lane-changing activities across all travel lanes, where the rightmost and its neighboring lanes often need to accommodate more lane changes and consequently experience more speed reduction (Rudjanakanoknad, 2012; Sun and Chen, 2017). Such lane-changing activities, typically classified as either mandatory or discretionary in nature, are exercised by drivers intending to exit the freeway or those avoiding the perceived speed reduction due to the spillback of off-ramp queues. Conceivably, the frequency and the distribution of these two types of lane-changing activities, varying with the freeway and off-ramp volumes, will characterize the nature and determine the degree of off-ramp queue impacts on the mainline segment.

To model the impacts of such lane-changing activities, it is essential to address the following three critical issues under the available

Table 1
List of key variables used in the OQI module.

a	Acceleration rate (m/s^2)
$C_{j,l}^{D}(k)$	Number of vehicles ***intending*** to make ***DLC*** from lanes j to l at time interval k
$C_{j,l}^{M}(k)$	Number of vehicles ***intending*** to make ***MLC*** from lanes j to l at time interval k
g^m	A minimum acceptable gap for lane changes (m)
$g_j^s(k)$	Minimal safety gap between vehicles in lane j at time interval k (m)
h^m	Minimum space headway (m)
L	Length of an off-ramp segment (m)
$L^H(k)$	The horizontal queue spillover length on mainline at time interval k (m)
L^v	Average vehicle length (m)
$N_j(k)$	Number of moving vehicles in lane j at time interval k
$N_j^E(k)$	Number of ***exiting*** vehicles in lane j at time interval k
$N_j^T(k)$	Number of ***through*** vehicles in lane j at time interval k
$n_{j,l}(k)$	Number of lane-changing vehicles from lanes j to l at time interval k
$n_j^1(k)$	Number of vehicles impacted by ***one*** moving-out vehicle ***to*** a slower-speed lane
$n_j^2(k)$	Number of vehicles impacted by ***one*** moving-in vehicle ***from*** a slower-speed lane
$n_{j,l}^D(k)$	Number of ***DLC*** vehicles from lanes j to l at time interval k
$n_{j,l}^M(k)$	Number of ***MLC*** vehicles from lanes j to l at time interval k
$p_{j,i}(k)$	***MLC*** probability of vehicle i on lane j at time interval k
$S_l(k)$	Remaining space of lane l for lane-changing vehicles at time interval k (vehicle)
Δt	Time interval duration (sec)
$t_j^f(k)$	The time duration that speeds of following vehicles of lane-changing vehicles are influenced (sec)
$v_j(k)$	Speed on lane j at time interval k (m/s) (from the speed-density relationship)
$v_j^1(k)$	Speed of lane j at time interval k under ***type-1*** impact (m/s)
$v_j^2(k)$	Speed of lane j at time interval k under ***type-2*** impact (m/s)
v^b	Backward shockwave speed (m/s)
$\overline{v}(k)$	Average speed across all freeway's travel lanes at time interval k (m/s)
$\overline{v}_j^*(k)$	Average speed of impacted vehicles in lane j during time interval k (m/s)
$q_j(k)$	Flow rate of lane j at time interval k (vph)
$q_j^{\epsilon}(k)$	Inflow rate of lane j at time interval k (vph)
$\widehat{q}^o(k)$	Inflow rate of the off-ramp at time interval k (vph)
$\widehat{q}^{\epsilon}(k)$	Flow rate ***joining*** to a tail of ***a queue spillover*** at time interval k (vph)
$x_{j,i}(k)$	Distance of vehicle i on lane j at time interval k from an off-ramp gore if no queue spillover exists and from a tail of a queue spillover, otherwise (m)
$y_{j,l}(k)$	Percentage of vehicles intending to make a ***DLC*** from lanes j to l at time interval k
λ	Longitudinal travel distance while making one lane change (m)
$\rho_j(k)$	The density of lane j at time interval k (prior to experience the lane changes by vehicles) (veh/km)
$\rho_j^*(k)$	The density of lane j at time interval k (after accommodating lane-changing vehicles) (veh/km)
ρ^{jam}	Jam density (veh/km)

traffic information: 1) the number of vehicles performing either type of lane-changing maneuvers in each travel lane; 2) the available space in each lane for such vehicles to complete their intended lane changes during each time interval; and 3) the resulting impacts on the freeway's traffic conditions.

All key steps in constructing the proposed OQI module for estimating ramp queue impacts are shown in Fig. 1; Table 1 summarizes the variable notations used hereafter in key formulations. Note that the control area on a freeway for studying the impacts of off-ramp queues typically ranges from the traffic sign that displays the off-ramp exit to the off-ramp gore or the end of the spillback queues.

As seen in Fig. 1, the OQI module based on the macroscopic traffic simulation notion, can approximate the freeway's traffic conditions in the presence of ramp queues during each time interval via the following sequential stages of computation and estimation:

Stage-1: estimating the number of intended lane-changing vehicles in each lane

Stage-2: computing the available roadway space for successful lane changes and the length of the off-ramp queue spillback

Stage-3: computing the impacts of the lane changes on the mainline' traffic speed

Stage-4: computing the density and flow rate of each lane

A detailed description of mathematical formulations used in each stage is presented in sequence below:

Stage-1: estimating the number of intended lane-changing vehicles in each lane

Compute the number of discretionary lane changes

Except for designated exit-only lanes, one can approximate the number of vehicles, $C^D_{j,l}(k)$, likely to perform DLC in each lane at time interval k as follows:

$$C^D_{j,l}(k) = N^T_j(k) \cdot y_{j,l}(k) \tag{1}$$

where, $N^T_j(k)$ is the total number of through vehicles within the subject lane segment at time interval k, and $y_{j,l}(k)$ denotes the fraction of through vehicles intending to make DLC from lanes j to l at time interval k.

Note that the number of vehicles that may have the desire to increase their speeds by changing to a fast-moving lane in the presence of off-ramp queues often varies with the following factors:

- speed difference between the subject and the target lanes;
- perceived difference in concentration between the subject and the target lanes;
- the average speed across all freeway's travel lanes;
- the perceived speeds and concentrations across all lanes beyond the interchange off-ramps; and
- the posted speed limit.

Hence, one shall calibrate a location-specific function with all the above factors for field implementation. The following function, calibrated in this study with the popular NGSIM dataset (FHWA, 2016), can serve as an alternative if field data for model development and application are not available. A detailed discussion of the estimation results for this nonlinear formulation (i.e., Eq. (3)) with regression (an adjusted R-square of 0.832) and its validation results are shown in Appendix A. Those parameters (i.e.,β_1, β_2, β_3, and β_4) may need to be recalibrated under the same model structure at different deployment locations if field data are available.

$$y_{j,l}(k) = \left(\frac{\exp\left(\overline{v}(k) - v_j(\mathrm{k}) - \mu_1\right)}{1+\exp\left(\overline{v}(k) - v_j(\mathrm{k}) - \mu_1\right)}\right)^{\beta_1}\left(\frac{\exp\left(v_l(\mathrm{k}) - v_j(\mathrm{k}) - \mu_2\right)}{1+\exp\left(v_l(\mathrm{k}) - v_j(\mathrm{k}) - \mu_2\right)}\right)^{\beta_2}\left(\frac{\left(\rho^{jam} - \rho_l(k)\right)}{\left|v_l(\mathrm{k}) - v_j(\mathrm{k})\right| + \xi}\right)^{\beta_3} e^{\delta\beta_4} \tag{2}$$

$$\ln y_{j,l}(k) = \beta_1 X_1 + \beta_2 X_2 + \beta_3 X_3 + \beta_4 \delta \tag{3}$$

where,

$X_1 = \ln\left(\frac{\exp\left(\overline{v}(k) - v_j(\mathrm{k}) - \mu_1\right)}{1+\exp\left(\overline{v}(k) - v_j(\mathrm{k}) - \mu_1\right)}\right)$; $\beta_1 = 0.191$ (*t-value* $= 16.2$);

$X_2 = \ln\left(\frac{\exp\left(v_l(\mathrm{k}) - v_j(\mathrm{k}) - \mu_2\right)}{1+\exp\left(v_l(\mathrm{k}) - v_j(\mathrm{k}) - \mu_2\right)}\right)$; $\beta_2 = 0.102$ (*t-value* $= 7.6$);

$X_3 = \ln\left(\frac{\left(\rho^{jam} - \rho_l(k)\right)}{\left|v_l(k) - v_j(k)\right| + \xi}\right)$; $\beta_3 = 0.456$ (*t-value* $= 12.5$);

$\delta = 1$, if changing to the right; $\delta = 0$, otherwise; $\beta_4 = -2.197$ (*t-value* $= -23.6$);

μ_1 is the average threshold of speed differences between subject lane and entire cross section from sample lane-changing drivers;

μ_2 is the average threshold of speed differences between subject and target lanes from sample lane-changing drivers; and

ξ is a very small value to prevent the denominator of the term, $(\rho^{jam} - \rho_l(k))/(\left|v_l(\mathrm{k}) - v_j(\mathrm{k})\right| + \xi)$, from equaling 0.

Note that those three terms in Eq. (2) are specified to reflect the following three consecutive conditions that will collectively work to motivate a driver to change lanes until actual completion of such a maneuver:

Condition-1: the current lane's speed less than the average speed of all travel lanes, and the difference exceeds a threshold;

Condition-2: the target lane's speed is higher than the speed of the current lane, and the difference exceeds a threshold;

Condition-3: the feasibility to complete a safe lane change that depends on the differences in both the speed and density between the subject and the target lanes.

Conceivably, the joint probability from those three conditions shall be the probability for a vehicle to successfully complete a discretionary lane change.

Compute the number of mandatory lane changes

With respect to the number of vehicles in each lane at time interval k intending to perform MLC, ($C_{j,l}^{M}(k)$), it is expected to be a function of the following factors:

- the distribution of off-ramp vehicles on the target highway segment, but not in the rightmost lane; and
- the distance to the off-ramp gore or the end of the spillback queue.

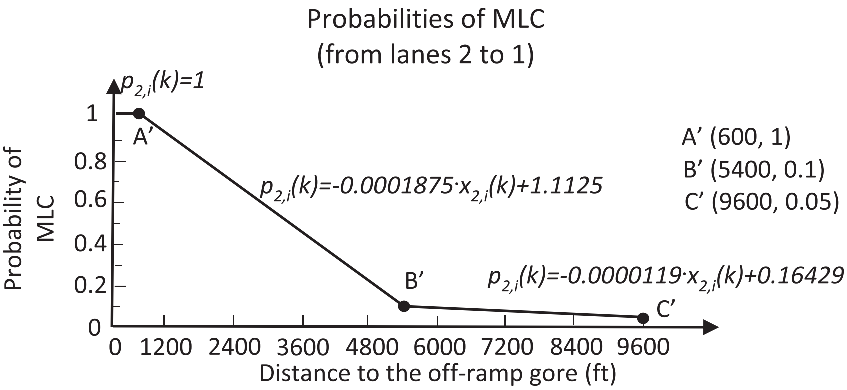

(a) Probability functions for MLC from lanes 2 to 1

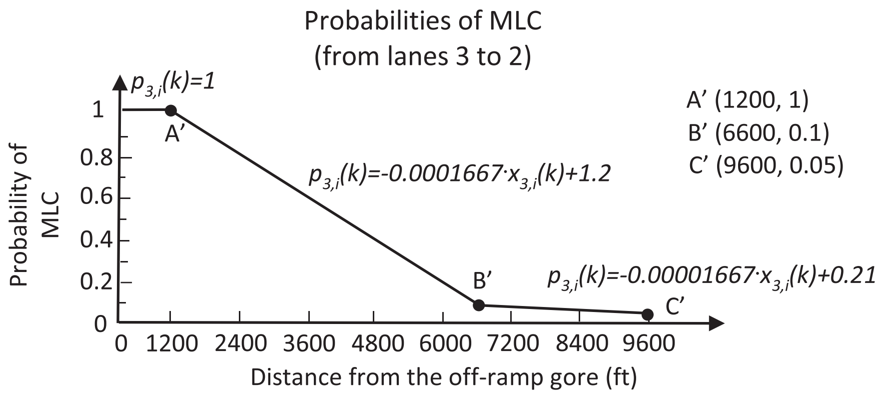

(b) Probability functions for MLC from lanes 3 to 2

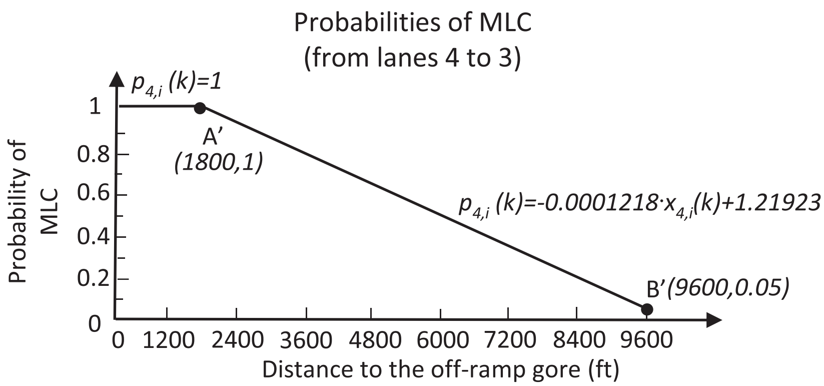

(c) Probability functions of MLC from lanes 4 to 3

Fig. 2. Probability functions for mandatory lane changes between neighboring lanes.

A mathematic expression for such vehicles over all travel lanes within the target area is shown below:

$$C^M_{j,l}(k) = \sum_{i=1}^{N_j^E(k)} p_{j,i}(k) \tag{4}$$

where, $p_{j,i}(k)$ denotes each vehicle's probability of exercising MLC.

With the assumption that all ramp-exiting vehicles before seeing the exit sign are distributed randomly among lanes and within each lane segment, one can approximate each vehicle's probability, $p_{j,i}(k)$, of exercising MLC with the following procedures derived from the field data and results by Pahl (1972).

Step-1: estimating the frequency of MLC between neighboring lanes from the following empirical function, calibrated by Pahl (1972):

$$F_{r,j,l} = w_{r,j,l} \Big/ \left[\widehat{N}_r \cdot 0.1135mile\right]$$

where, $F_{r,j,l}$ is the frequency per mile of exiting-vehicles changing from lane j to lane l in zone r; $w_{r,j,l}$ is the number of exiting-vehicle changes from lane j to lane l in zone r; and $\widehat{N}_r$ is the total number of exiting vehicles in zone r.

Step-2: converting the estimated lane-changing frequency between neighboring lanes to Fig. 2 (derived from Pahl's work, 1972), showing the probability of changing lanes at different distances from the off-ramp gore.

Step-3: compute the MLC probability for vehicles at a given distance from the off-ramp gore at each interval k with the above figures or from their mathematical expressions shown below:

$$p_{j,i}(k) = \begin{cases} 1, if 0 \le x_{j,i}(k) < \dfrac{\alpha_j^2 - 1}{\alpha_j^1} \\ -\alpha_j^1 \cdot x_{j,i}(k) + \alpha_j^2, if \dfrac{\alpha_j^2 - 1}{\alpha_j^1} \le x_{j,i}(k) < \dfrac{\alpha_j^2 - \alpha_j^4}{\alpha_j^1 - \alpha_j^3} \\ -\alpha_j^3 \cdot x_{j,i}(k) + \alpha_j^4, if \dfrac{\alpha_j^2 - \alpha_j^4}{\alpha_j^1 - \alpha_j^3} \le x_{j,i}(k) \le 9,600(ft) \end{cases} \tag{5}$$

where,

$p_{j,i}(k)$ is the lane-changing probability of vehicle i on lane j at time interval k;

$x_{j,i}(k)$ is the distance of vehicle i on lane j at time interval k from an off-ramp gore if no queue spillover exists and from the tail of a queue spillover (ft), otherwise; and

$\alpha_j^1, \alpha_j^2, \alpha_j^3, \text{and} \alpha_j^4$ are parameters for lane j.

Note that with the above procedures for MLC probability and the assumption that all such vehicles are distributed uniformly in each lane, one can approximate the total number of MLC vehicles in each lane over time from the macroscopic perspective with Eq. (4).

Stage-2: Computing the available roadway space for successful lane changes and the length of the off-ramp queue spillback

Note that a driver's lane-changing exercise can be accomplished only if the target lane at time interval k has sufficient space for doing so. Hence, by assuming that the space headways on each lane follow a normal distribution, one can approximate the available space for lane changes, $S_l(k)$, with the following expression:

$$S_l(k) = \begin{cases} N_l(k) \cdot \sum_{z=1}^{L\rho^{jam} - N_l(k)} z \cdot p\left(z\left(\dfrac{v_l(k)^2 - v_j(k)^2}{2a} + L^v\right) \le g < (z+1)\left(\dfrac{v_l(k)^2 - v_j(k)^2}{2a} + L^v\right)\right), if\, v_l(k) > v_j(k) \\ N_l(k) \cdot \sum_{z=1}^{L\rho^{jam} - N_l(k)} z \cdot p(zg^m \le g < (z+1)g^m), otherwise \end{cases} \tag{6}$$

where, $N_l(k)$ is the number of moving vehicles in the target lane l within the study area, which can be estimated with the lane density and its length not occupied by the spillback queues. The probability, $p(zg^m \le g < (z+1)g^m)$, reflects the available gaps that can accommodate z vehicles changing from a higher-speed lane to a lower one. In contrast, only those gaps on the target lane, exceeding the safety distance, $(v_l(k)^2 - v_j(k)^2)/2a + L^v$, can be taken by vehicles to move from a slower lane to the faster-moving one.

Note that the time-varying length, $L^H(k)$, of spillover queues on the freeway mainline, used for estimating the available gaps for vehicles from its left lanes to conduct MLC, can be expressed as follows:

$$L^H(k) = L^H(k-1) + h^m \cdot \left(\widehat{q}^{\epsilon}(k-1) - \widehat{q}^o\left(k - \lfloor t^b/\Delta t \rfloor - 1\right)\right) \cdot \Delta t/3600 \tag{7}$$

$$t^b = L^H(k-1)/v^b \tag{8}$$

where, the second term in Eq. (7) shows the queue length variation based on the number of vehicles joining the queues and those flowing to the off-ramp. Note that Eq. (8) is for computing the time lag, t^b, for the off-ramp queue discharging shockwave at the speed of v^b to reach the end of the spillback queues.

Conceivably, the distributions of DLC and MLC from the microscopic perspective may vary across freeway lanes. However, for assessing their collective impacts of such lane changes on the freeway segment's overall traffic conditions, it is reasonable to assume that each of such changing vehicles has the same opportunity to do so under the given available space headways. Hence, one can approximate the number of vehicles completed MLC, ($n^M_{j,l}(k)$, and DLC ($n^D_{j,l}(k)$) based on their ratios and with the following expressions:

$$n^M_{j,l}(k) = \min\left\{ S_l(k)\bullet\frac{C^M_{j,l}(k)}{\sum_{\widehat{j}\in\Omega_l}\left(C^D_{\widehat{j,l}}(k) + C^M_{\widehat{j,l}}(k)\right)}, C^M_{j,l}(k)\right\} \tag{9}$$

$$n^D_{j,l}(k) = \min\left\{ S_l(k)\bullet\frac{C^D_{j,l}(k)}{\sum_{\widehat{j}\in\Omega_l}\left(C^D_{\widehat{j,l}}(k) + C^M_{\widehat{j,l}}(k)\right)}, C^D_{j,l}(k)\right\} \tag{10}$$

where, Ω_l is the set of neighboring lanes of lane l.

Naturally, the total number of lane-changing vehicles,$n_{j,l}(k)$, can be shown with Eq. (11).

$$n_{j,l}(k) = n^M_{j,l}(k) + n^D_{j,l}(k) \tag{11}$$

Stage-3: Computing the impacts of the lane changes on the mainline' traffic speed

For each lane segment near the off-ramp, its average speed is likely to be impacted by the following two types of lane-changing activities: moving into the slower-moving neighboring lane to get off the ramp (denoted as Type-1), and discretionary lane changes by vehicles from a neighboring lane to increase speed (named Type-2). In the case of Type-1, the lane-changing vehicles in the original lane need to first decelerate to adapt to the speed of the target lane. As a result, their following vehicles in the original lane will be forced to first decelerate to accommodate the speed of the lane-changing vehicle, and then accelerate to get back to their original speed. In the case of Type-2, the following vehicles in the receiving lane are compelled to adjust their speeds due to the vehicle changing from a slower neighboring lane.

For Type-1 impact, each vehicle, prior to changing to the slower-speed lane, is expected to decelerate to the same speed as the target lane (denoted as lane l). Hence, let $t^f_j(k)$ and $\Delta\eta_{j,l}(k)$ be defined as the required time duration and resulting travel distance for the subject lane vehicles to decelerate from its current speed, $v_j(k)$, to the target lane speed, $v_l(k)$, and then recover to the same speed after the lane-changing vehicle completed its maneuver. And $\Delta\theta_j(k)$ denotes the average space headway between vehicles on the subject lane at time interval k. Then, one can approximate the number of vehicles ($n^1_j(k)$) on the subject lane impacted by one such lane-changing vehicle as $\Delta\eta_{j,l}(k)/\Delta\theta_j(k)$, where,

$\Delta\eta_{j,l}(k) = t^f_j(k)\bullet(v_j(k) - v_l(k))/2$, for $v_j(k) > v_l(k)$;

$\Delta\theta_j(k) = (1000/\rho_j(k)) - L^v - g^s_j(k)$;

$g^s_j(k)$ is the minimum safety gap between vehicles in lane j at time interval k;L^v is the average vehicle length; and $\rho_j(k)$ is the density of the subject lane.

As for the resulting impacts on the subject lane's average speed, it depends on both the total estimated lane changes ($n_{j,l}(k)$) for the subject lane during interval k, and the number of vehicles impacted by each of such lane changes ($n^1_j(k)$). From the macroscopic perspective, one can naturally approximate the resulting average speed under such Type-1 lane-changing vehicles as follows:

$$v^1_j(k) = \begin{cases} \overline{v}^*_j(k) & \text{, if } n_{j,l}(k)\bullet n^1_j(k) \geq N_j(k) \\ [\overline{v}^*_j(k)\bullet n_{j,l}(k)\bullet n^1_j(k) + v_j(k)\bullet\left(N_j(k) - n_{j,l}(k)\bullet n^1_j(k)\right)]/N_j(k), & \text{otherwise} \end{cases} \tag{12}$$

where the condition, $n_{j,l}(k)\bullet n^1_j(k) \geq N_j(k)$, indicates that all subject lane vehicles, ($N_j(k)$), are subject to the speed impacts due to those Type-1 lane changes ($n_{j,l}(k)\bullet n^1_j(k)$); and the resulting average lane speed, $v^1_j(k)$, shall equal $\overline{v}^*_j(k)$ shown in Eq. (13):

$$\overline{v}^*_j(k) = \left[t^f_j(k)\bullet(v_l(k) + v_j(k))\right/2 + \left(\Delta t - t^f_j(k)\right)\bullet v_j(k)]/\Delta t, v_j(k) > v_l(k) \tag{13}$$

In Eq. (13), $(v_l(k) + v_j(k))/2$ is the average speed of lane-changing vehicles during deceleration, and $t^f_j(k)$ is the deceleration duration. In addition, $v_j(k)$ is the traveling speed of lane-changing vehicles before deceleration. As such, $\overline{v}^*_j(k)$ is the weighted average speed of the above two speed values. Otherwise, $v^1_j(k)$ can be approximated with the weighted speed average of both vehicles free from and subject to the impact of Type-1 lane-changing vehicles.

Note that by following the same logic, one can also derive the average speed of lane j, subjected to the Type-2 impacts of moving-in vehicles from a slower-speed lane, as shown in Eq. (14):

$$v_j^2(k) = \begin{cases} \overline{v}_j^*(k) & , \text{ if } n_{l,j}(k) \cdot n_j^2(k) \geq N_j(k) \\ \left[\overline{v}_j^*(k) \cdot n_{l,j}(k) \cdot n_j^2(k) + v_j(k) \cdot \left(N_j(k) - n_{l,j}(k) \cdot n_j^2(k)\right)\right] \Big/ N_j(k), & \text{otherwise} \end{cases} \tag{14}$$

where, $n_j^2(k)$ denotes the number of vehicles in lane j impacted by one moving-in vehicle from a slower-speed lane.

In addition, in terms of the receiving lane, after the lane-changing vehicles complete the changes, the density of the lane will increase. As a result, the average speed of the receiving lane will decrease. In other words, all vehicles in the receiving lane will be affected. With respect to the original lane, its density will decrease after the lane-changing vehicles leave the lane. Then, the average speed of the original lane will increase.

Stage-4: Computing the density and flow rate of each lane

With the estimated number of lane-changing vehicles, one can update the resulting lane density and densities at the current time interval with the following expressions:

$$\rho_j^*(k) = \rho_j(k) + \frac{1000}{\left(L - L^H(k) - (j-1) \cdot \lambda\right)} \left(n_{l,j}(k) - n_{j,l}(k)\right) \tag{15}$$

$$q_j(k) = \rho_j^*(k) * \min\left[v_j^1(k), v_j^2(k)\right] \cdot 3.6 \tag{16}$$

$$\rho_j(k+1) = \rho_j^*(k) + \frac{\Delta t}{3.6 \cdot \left(L - L^H(k+1) - (j-1)\lambda\right)} \left(q_j^e(k) - q_j(k)\right) \tag{17}$$

Eq. (16) presents the flow rates determined by the density after accommodating those lane-changing vehicles (i.e., $\rho_j^*(k)$) and the minimum of speeds under Type-1 and Type-2 impacts (i.e., $min\left[v_j^1(k), v_j^2(k)\right]$). If such vehicles are concurrently influenced by those vehicles changing from a slower lane (i.e., Type-1 impact) and vehicles changing to a slower lane (i.e., Type-2 impact), then they shall adopt to the lower one between these two types of vehicles.

2.2. The OQI module validation

Experimental site

Fig. 3 illustrates the freeway segment in Taiwan for the OQI module evaluation and the locations of its six vehicle detectors (VDs), as well as one electric toll collection (ETC) sensor for data collection. Both the speeds and flow rates collected from 15:00 to 21:00 on March 7, 2019 are used as the dataset for calibration. The same data set available on March 14, 2019 serves as the basis for evaluating the calibrated module's performance.

Fig. 4 shows the observed time-varying flow rates on the freeway segment and to the off-ramp in the dataset for validation. Noticeably, the maximum freeway flow rate was up to 10,100 vph, and the inflow rates to the off-ramp varied between 1,350 vph to 2,400 vph during the same period. Fig. 5 presents the time-varying average lane speeds from VDs located between 363.8 k and 365.3 k.

Evaluation results

Fig. 6 shows the numbers of estimated DLC. Over most time intervals, the frequencies of DLC from lane 4 to lane 5 are lower than those from lanes 2 to 3 and from lanes 3 to 4, because the impacts of the off-ramp queue spillovers on the inner lanes are less than those on the outer lanes. Moreover, the number of DLC is related to the speed difference between the current and target lanes. For example, the number of DLC from lanes 2 to 3 spiked at a period from 17:30 to 18:00 (i.e., mark A) because the speed of lane 2 has decreased since 17:30, but lane 3′s speed did not drop until 18:00 (see Fig. 9 (b) and (c)). The same phenomena can be observed from the number of DLC from lanes 3 to 4 between 18:00 and 18:20 (i.e., mark B). Additionally, Fig. 7 shows the numbers of estimated MLC. Conceivably, the numbers of MLC by exiting vehicles in the outer lanes are higher than the inner lanes because the exiting vehicles need to laterally traverse all its right-side lanes to reach the off-ramp. As a result, the MLC from lane 2 to lane 1 exhibits the highest frequency. Moreover, the numbers of MLC peaked at a period from 17:00 to 18:00 and then decrease afterward. Such a trend is

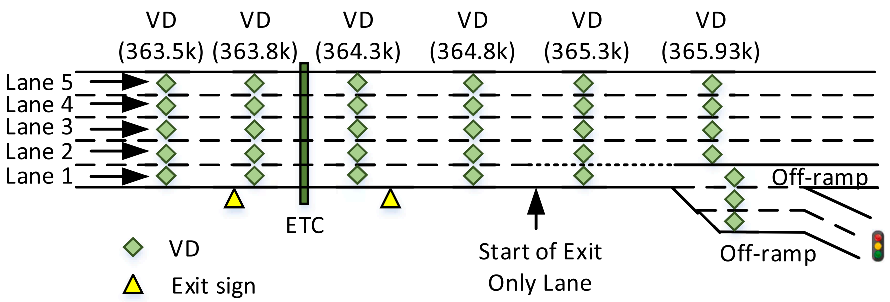

Fig. 3. Locations of the detectors and the ETC station.

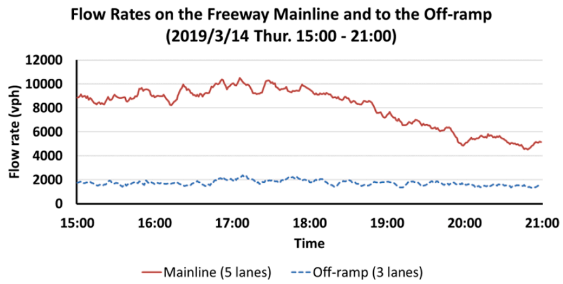

Fig. 4. Time-varying flow rates on the freeway mainline and to the off-ramp.

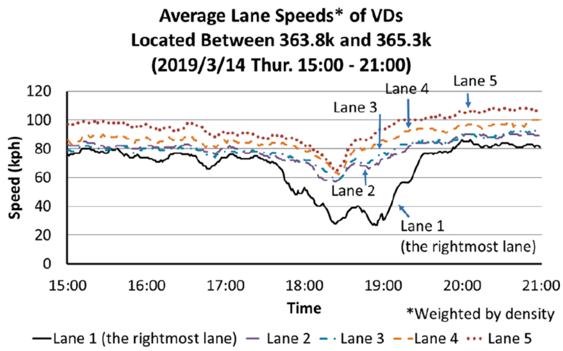

Fig. 5. Time-varying average lane speeds.

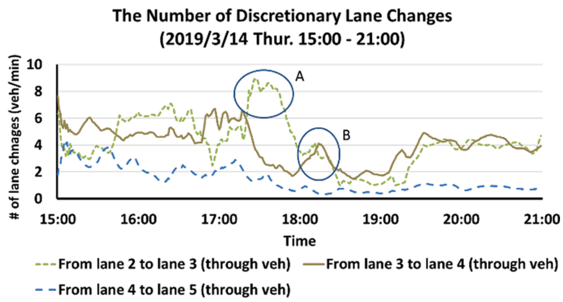

Fig. 6. The number of discretionary lane changes estimated with the proposed module.

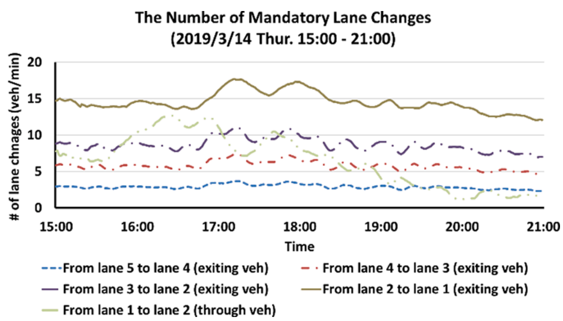

Fig. 7. The number of mandatory lane changes estimated with the proposed module.

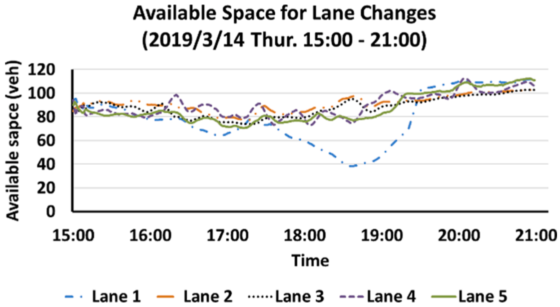

Fig. 8. Available space for lane changes estimated with the proposed module.

consistent with the evolution pattern of the exiting volumes (see Fig. 4).

Fig. 8 shows the available space for lane-changing vehicles. Because of the queue spillover, the available space in lane 1 (the outermost lane) decreases to about 40 vehicles around 18:30 when the length of the queue spillover reaches the longest point (about 1,500 m). However, the available space for lane-changing vehicles is larger than the numbers of DLC and MLC. Therefore, all the exiting vehicles can still change to the outermost lane before reaching the off-ramp goal or the tail of the queue spillover.

To assess the calibrated module's performance under different traffic conditions, Table 2 presents the statistical test results with respect to the predicted speeds for both the peak (16:30–19:30) and off-peak (15:00–16:30 & 19:30–21:00) hours, based on the mean absolute error (MAE), mean absolute percentage error (MAPE), and Theil's Inequality Coefficient, a well-recognized test in econometrics to test a model's prediction power (Koutsoyiannis, 1973). As shown in Eq. (18), this coefficient can concurrently measure the following two types of errors: 1) the discrepancy between prediction values and field data caused by the difference between their means; and 2) the discrepancy between prediction values and field data caused by the difference between their variances.

$$Theil\grave{}sInequalityCoefficient : U = \sqrt{\frac{\sum (P_i - A_i)^2/n}{\sum A_i{}^2/n}} 0 \leq U \leq \infty \tag{18}$$

where, P_i are predicted values; A_i are actual values; n is the number of data points; and the model is viewed to attain perfect forecasts if $U = 0$ (i.e., $P_i = A_i$). Noticeably, the module, after calibrated to minimize the differences between the field-collected and simulated per-lane flowrate and per-lane speed, can reasonably capture the complex off-ramp queue impacts on the freeway's speed and flow rate as well as their distributions across lanes. Table 3 shows the list of key parameter settings used in the OQI module. All the parameters have been calibrated for the study site by minimizing the differences between the field-collected and simulated per-lane flow rate and per-lane speed.

All MAPEs for all travel lanes' speeds during both peak and off-peak hours are less than 5%, except the 5.5% for lane-1 during the peak hours. This is further supported by the resulting MAEs, where the differences between the detected and predicted speeds across all five lanes during both peak and off-peak hours are less than 5 kph, as shown in Table 2. Additionally, Fig. 9 shows that the model can reproduce the speed evolution at the acceptable level of accuracy.

Fig. 10 further illustrates the distributions of predicted errors with respect to the speed by the freeway travel lane during both peak (Fig. 10 (a)) and off-peak hours (Fig. 10 (b)), mostly less than 5 kph. The results with Theil's Inequality Coefficient also reveal that the module's prediction errors are mostly less than 0.05, as shown in Table 2. Moreover, traffic flows on lane-1 (i.e., the rightmost lane), as expected, are observed to suffer the most impact by the off-ramp queue spillback during the peak hours. Evidently, the results of those three test statistics for the speed of lane-1 are all relatively larger than for all other lanes. For example, the MAPE of the lane-1′s speed during peak hours is 5.5%, but the same statistics for all others are less than 3.5% (see Table 2). In addition, the off-ramp queue spillback on the freeway's rightmost lane in the peak hours will inevitably intensify the lane-changing behaviors. Hence, the predicted discrepancies on most lanes during the peak hours are naturally larger than those in the off-peak hours. For example, the MAE for the speed on lane-1 during the peak hours is 3.35 kph, much higher than the 1.92 kph for the off-peak periods.

Table 4 highlights the evaluation results with respect to the freeway mainline outflow rate under the same performance test statistics during the same peak and off-peak periods. Noticeably, the MAPEs for the flow rate on all travel lanes are less than 10%, varying between the lowest of 4.9% on lane-5 in peak hours and the highest of 8.7% on lane-2 during the off-peak hours. Furthermore, as shown in Table 4, the MAPE for flow rates in the peak hours has the highest value on lane-2 (i.e., 7.5%), and the lowest for lane-5 (i.e., 4.9%) because the lane closer to the rightmost lane tend to experience more interference from the off-ramp queue spillover. In addition, the predicted discrepancies with respect to the flow rates (vehicles per minute on each lane) lie within the range of less than three vehicles per minute for all travel lanes during the entire period. The proposed module's potential for predicting the flow rate variation and evolution on the freeway segment due to off-ramp flows is also confirmed from the test results with the Theil's Inequality Coefficient, as mostly within the range of 0.1. This is consistent with the distribution of predicted discrepancies with respect to the freeway mainline outflow rate by lane shown in Fig. 11 over both the peak and off-peak hours. In addition, Fig. 12 further shows the flow rate evolutions.

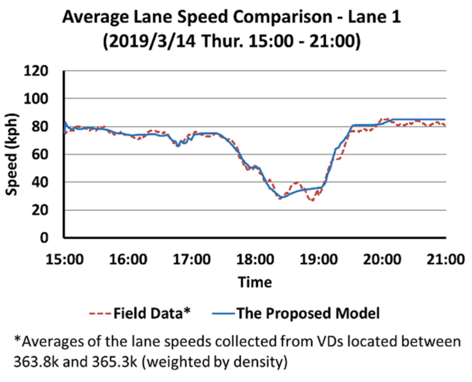

(a) Lane 1

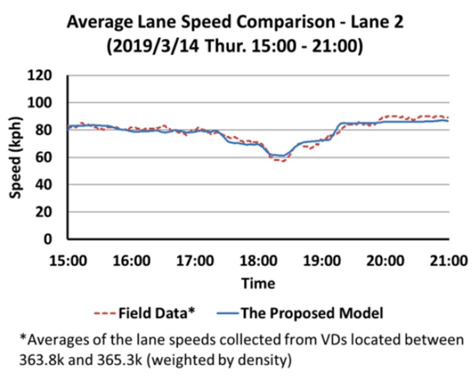

(b) Lane 2

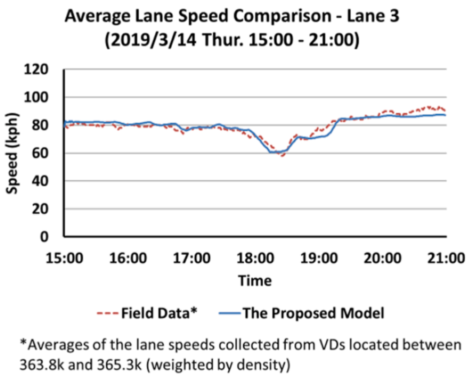

(c) Lane 3

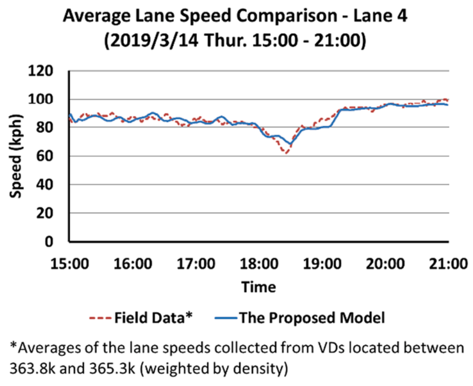

(d) Lane 4

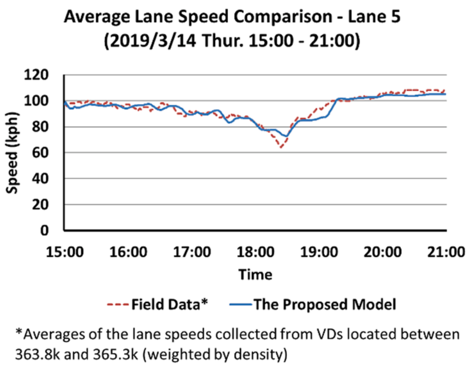

(e) Lane 5

Fig. 9. Average lane speed comparison.

Queue length prediction

Since the core of this study is to reflect the impacts of off-ramp queue spillovers on the freeway's traffic condition, evaluating the predicted accuracy of the OQI module with respect to the time-varying queue length is an essential task. Fig. 13 shows the time-varying off-ramp queues estimated by the module and the discrete queues observed from the field data. Note that the field-developed off-ramp queue length is observable only when it occupies or exceeds the deployed VD. An occupancy threshold of 25% is used to determine whether the queue has reached the VDs or not (Liu et al., 2007). As such, the evolution of the field-detected queue length can only be recorded with its times to reach the set of deployed queue detectors.

Due to the discrepancy in data nature between the field-observed and module-produced queues, this study has adopted two non-parameter tests, *Mann-Whitney U* and *Siegel-Tukey* tests, to evaluate if the differences between these two sets of queues are statistically insignificant. The results from both tests indicate that these two graphical patterns shown in Fig. 13 are statistically indifferent at the 5% significant level.

Table 2
Comparison between the detected and predicted freeway speeds.

Test statistics	Lane No.				
	1	2	3	4	5
Theil's Inequality Coefficient					
Peak hours	0.062	0.033	0.036	0.038	0.044
Off-peak hours	0.028	0.028	0.032	0.023	0.024
Mean Absolute Error (MAE) (kph)					
Peak hours	3.35	2.05	2.10	2.50	2.90
Off-peak hours	1.92	2.01	2.23	1.75	2.06
Mean Absolute Percentage Error (MAPE)					
Peak hours	5.5%	2.9%	2.8%	3.2%	3.4%
Off-peak hours	2.4%	2.3%	2.8%	2.3%	2.0%

Table 3
Key parameters of the off-ramp queue impact module.

Parameter	Value
a	1.6 m/s^2
g^m	10 m
h^m	7.7 m
L^v	5.2 m
v^b	3.3 m/s
$\beta_1^*, \beta_2^*, \beta_3^*, \beta_4^*$	0.211, 0.112, 0.486, −2.23
λ	25 m
ρ^{jam}	130 veh/km/lane

*The parameters are recalibrated by the field data from the case study site.

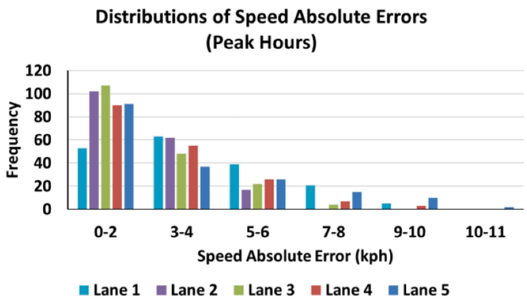

(a) Peak hours

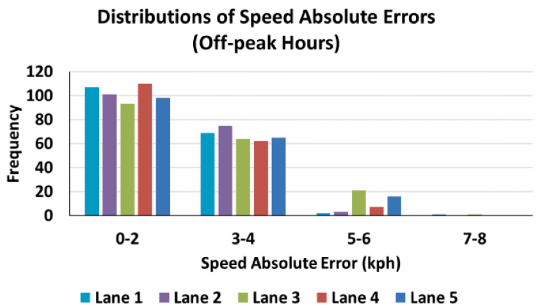

(b) Off-peak hours

Fig. 10. Distributions of speed absolute errors.

Table 4
Validation results of freeway mainline outflow rates.

Test statistics	Lane No.				Cross Section[a]
	2	3	4	5	
Theil's Inequality Coefficient					
Peak hours	0.092	0.084	0.082	0.058	0.115
Off-peak hours	0.097	0.071	0.068	0.076	0.172
Mean Absolute Error (MAE) (veh/min)					
Peak hours	1.41	1.79	2.13	1.51	3.73
Off-peak hours	1.37	1.32	1.58	1.34	3.84
Mean Absolute Percentage Error (MAPE)					
Peak hours	7.5%	6.9%	6.5%	4.9%	3.0%
Off-peak hours	8.7%	5.7%	5.2%	6.4%	4.4%

[a] Outflow rate for the entire freeway mainline segment.

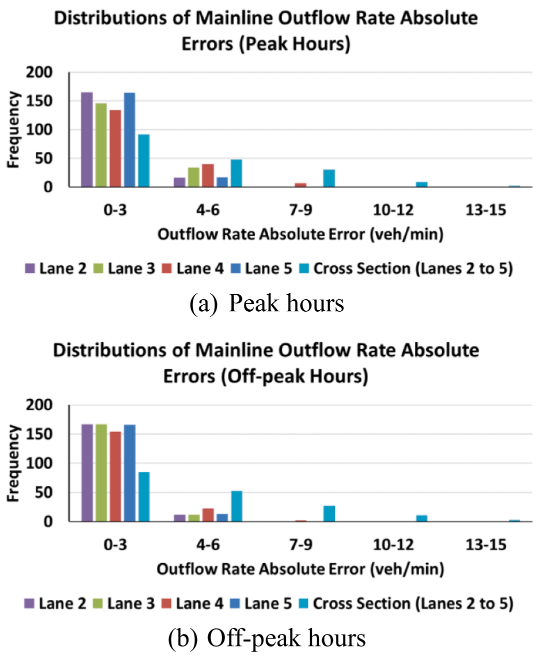

Fig. 11. Distributions of mainline outflow rate absolute errors.

2.3. Sensitivity analysis

Recognizing the critical role of the proposed OQI's embedded parameters (i.e., $\beta_1, \beta_2, \beta_3, \beta_4, g^m, h^m, L^v$, and a), this study has further conducted their sensitivity analyses at the following levels:$\pm$20%, $\pm$40%, and $\pm$60% variation of their initial values. Key findings from such results (shown in Figs. 14–21) are summarized below:

1. Decreasing β_1 will increase the percentage of drivers intending to conduct discretionary lane changes to faster lanes (i.e., lanes 4 and 5), and consequently cause speed reduction on lanes 4 and 5 (see Fig. 14), but not on the lane outflow rates (see Fig. 15). For example, when β_1 decrease by 60%, the lane-5 speed drops by 8% (see Fig. 14), but its outflow rate received a 4.7% increase (see Fig. 15). On the contrary, increasing β_1 (i.e., decreasing the discretionary lane- changing probability) will reduce the speeds on the lane-2 and lane-3 and concurrently decrease the lane outflow rates. For instance, both the speed and flow rate for lane-2 will drop by 3.5% when β_1 increases by 60%. Similar sensitivity patterns also exist for β_2 and β_3.
2. As shown in Figs. 16 and Fig. 17, the lane outflow rates and speeds are relatively insensitive to different values for β_4. Such results reveal that drivers generally prefer to stay on the left lane within the off-ramp weaving segment, especially during peak hours, even though their intentions to change to the right lane of the faster-speed lane may increase with the increased specified value for β_4.
3. As shown in Fig. 18, a decrease in the minimum acceptable gap for lane changes, g^m, will result in a reduction in the average lane speeds. The reason lies in that vehicles forcefully merging into a smaller gap will cause more impacts on their following vehicles in the receiving lane. For example, a reduction of 60% in g^m will reduce the lane-1 speed by 4.6%. Moreover, this parameter can reflect the aggressiveness of drivers in the lane-changing maneuver (i.e., a smaller g^m represents a more aggressive behavior).

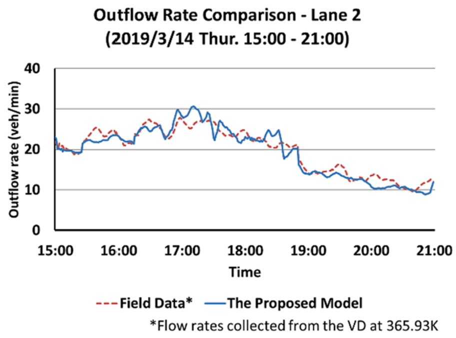

(a) Lane 2

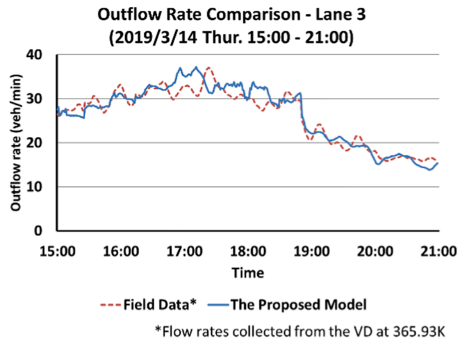

(b) Lane 3

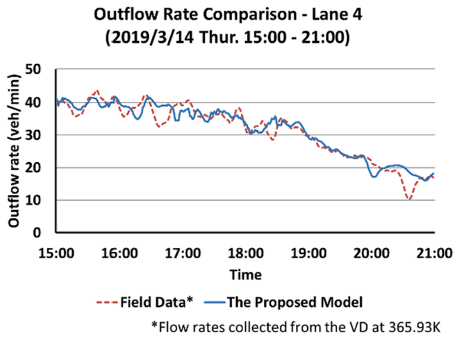

(c) Lane 4

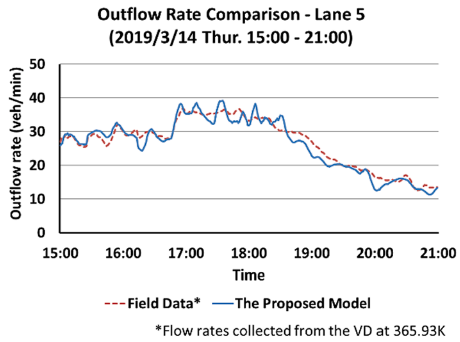

(d) Lane 5

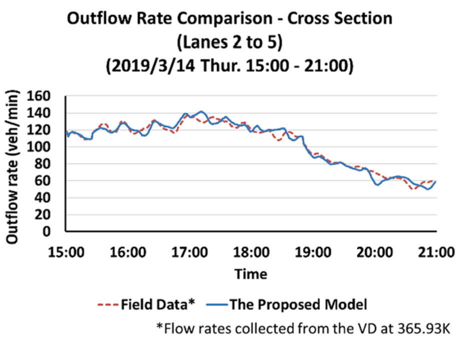

(e) Cross section (Lanes 2 to 5)

Fig. 12. Freeway mainline outflow rate comparison.

4. As shown in Fig. 19, when decreasing h^m (i.e., minimum space headway), the average lane speeds will increase. The reason is that a decrease in the minimum space headway will result in a shorter length of queue spillover, and thus improve the lane speeds. For example, the speed of lane 1 increases by 18.4% under the scenario of a 60% reduction of h^m. On contrast, increasing the minimum space headway indicates an increase in the length of the queue spillover and a higher probability for such queues to interfere with the mainline flows and thus reduce the lane speeds. The lane-1 speed, for instance, decreases by 12.7% if the minimum space headway increases by 60%.
5. A longer average vehicle length (i.e., L^v) will inevitably result in lower average lane speeds, because the traffic flows need to have larger gaps to accommodate such lane-changing vehicles. Furthermore, the lane-changing maneuver by vehicles of a longer length will certainly pose more significant impacts on traffic on the receiving lanes and consequently further reduce their speeds. For example, all lanes exhibit a speed reduction by 2.7% to 5.3% when the average vehicle length increases by 60% (see Fig. 20).
6. As shown in Fig. 21, a decrease value for the parameter, a (i.e., acceleration rate) will cause a reduction in the lane speed, because such vehicles need larger gaps in the target lane for safe lane changes, as reflected in the reduced number of lane changes. Moreover, the lane-changing maneuvers by vehicles of a lower acceleration rate will impact more significantly on the receiving lane's speed. For example, the speeds of lanes 1 to 5 drop by 4.3%, 5.4%, 4.6%, 5.2%, and 1.7%, respectively, when the acceleration rate decreases by 60% (see Fig. 21).

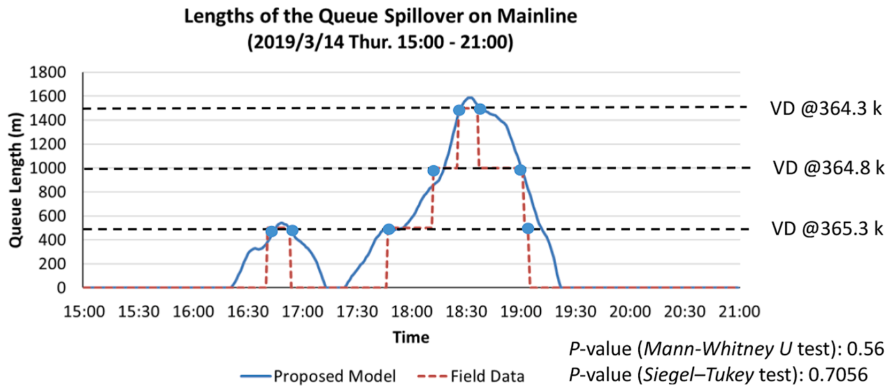

Fig. 13. Comparison between the field-observed and module-produced time-varying queues.

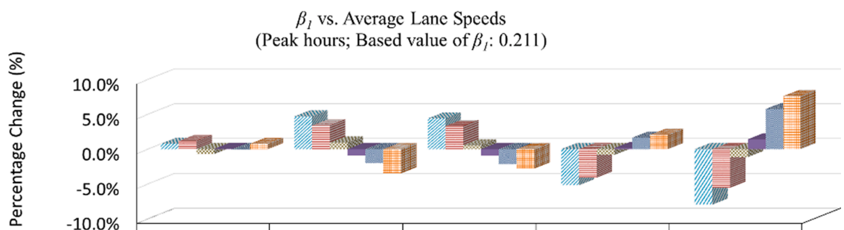

	Lane 1	Lane 2	Lane 3	Lane 4	Lane 5
β_1 decreased by 60%	0.8%	4.7%	4.4%	-5.2%	-8.0%
β_1 decreased by 40%	1.2%	3.4%	3.3%	-4.1%	-5.6%
β_1 decreased by 20%	-0.7%	0.9%	0.6%	-0.8%	-1.1%
β_1 increased by 20%	0.0%	-0.9%	-0.9%	0.2%	1.4%
β_1 increased by 40%	0.0%	-2.0%	-2.1%	1.6%	5.8%
β_1 increased by 60%	0.8%	-3.5%	-2.8%	2.1%	7.6%

Lanes

Fig. 14. Relative changes in the average lane speed with respect to β_1.

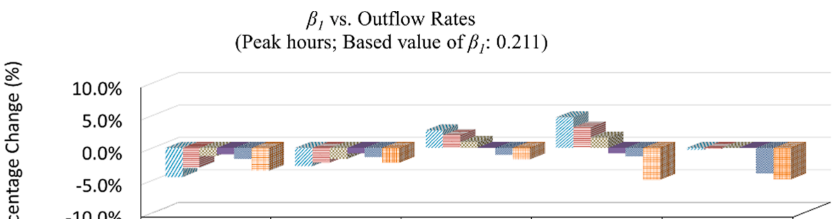

	Lane 2	Lane 3	Lane 4	Lane 5	Cross Section (Lanes 2 to 5)
β_1 decreased by 60%	-4.5%	-2.8%	2.7%	4.7%	-0.3%
β_1 decreased by 40%	-3.1%	-2.2%	2.0%	3.2%	-0.1%
β_1 decreased by 20%	-1.2%	-1.7%	0.9%	1.6%	0.0%
β_1 increased by 20%	-1.0%	-0.8%	0.0%	-0.8%	0.0%
β_1 increased by 40%	-1.7%	-1.4%	-1.1%	-1.3%	-3.9%
β_1 increased by 60%	-3.5%	-2.3%	-1.8%	-4.9%	-4.8%

Lanes

Fig. 15. Relative changes in the outflow rate with respect to β_1.

7. Compared to the other parameters, the average lane speed is more sensitive to the variation of h^m (see in Fig. 14 and Figs. 17–21). The likely reason is that the minimum space headway will directly affect the off-ramp queue spillover length that is one of the main factors causing traffic breakdown in the freeway off-ramp segment.
8. Except for h^m (i.e., minimum space headway), the average speeds are relatively stable with respect to the parameters as long as their variation is less than 20%.

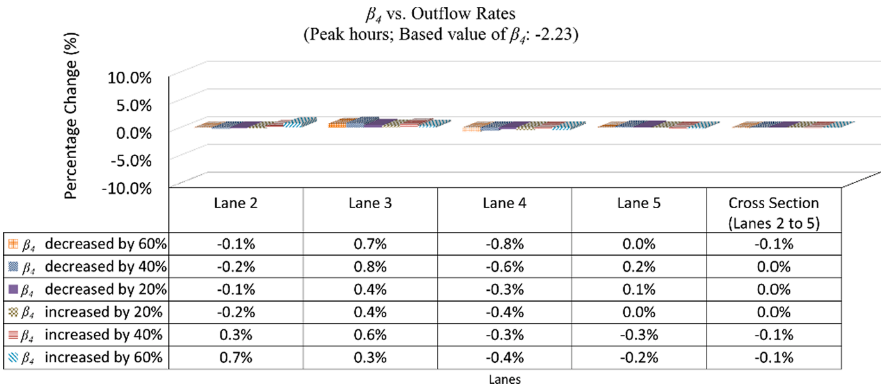

	Lane 2	Lane 3	Lane 4	Lane 5	Cross Section (Lanes 2 to 5)
β_4 decreased by 60%	-0.1%	0.7%	-0.8%	0.0%	-0.1%
β_4 decreased by 40%	-0.2%	0.8%	-0.6%	0.2%	0.0%
β_4 decreased by 20%	-0.1%	0.4%	-0.3%	0.1%	0.0%
β_4 increased by 20%	-0.2%	0.4%	-0.4%	0.0%	0.0%
β_4 increased by 40%	0.3%	0.6%	-0.3%	-0.3%	-0.1%
β_4 increased by 60%	0.7%	0.3%	-0.4%	-0.2%	-0.1%

Fig. 16. Relative changes in the outflow rate with respect to β_4.

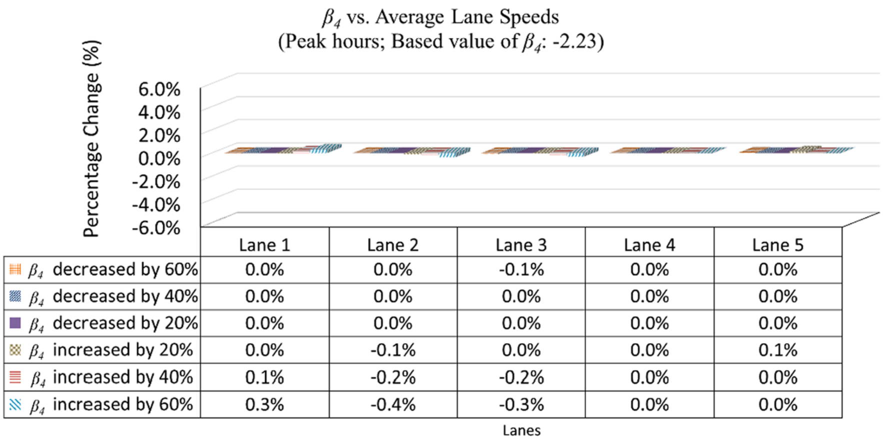

	Lane 1	Lane 2	Lane 3	Lane 4	Lane 5
β_4 decreased by 60%	0.0%	0.0%	-0.1%	0.0%	0.0%
β_4 decreased by 40%	0.0%	0.0%	0.0%	0.0%	0.0%
β_4 decreased by 20%	0.0%	0.0%	0.0%	0.0%	0.0%
β_4 increased by 20%	0.0%	-0.1%	0.0%	0.0%	0.1%
β_4 increased by 40%	0.1%	-0.2%	-0.2%	0.0%	0.0%
β_4 increased by 60%	0.3%	-0.4%	-0.3%	0.0%	0.0%

Fig. 17. Relative changes in the average lane speed with respect to β_4.

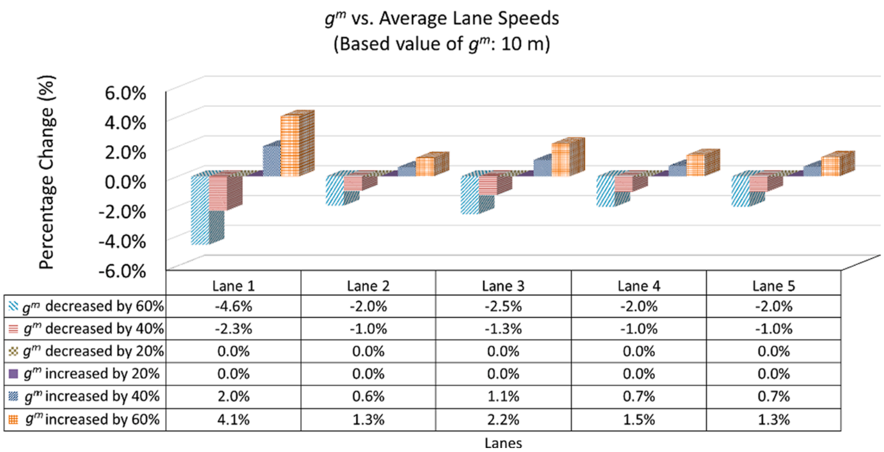

	Lane 1	Lane 2	Lane 3	Lane 4	Lane 5
g^m decreased by 60%	-4.6%	-2.0%	-2.5%	-2.0%	-2.0%
g^m decreased by 40%	-2.3%	-1.0%	-1.3%	-1.0%	-1.0%
g^m decreased by 20%	0.0%	0.0%	0.0%	0.0%	0.0%
g^m increased by 20%	0.0%	0.0%	0.0%	0.0%	0.0%
g^m increased by 40%	2.0%	0.6%	1.1%	0.7%	0.7%
g^m increased by 60%	4.1%	1.3%	2.2%	1.5%	1.3%

Fig. 18. Relative changes in the average lane speed with respect to g^m.

3. The integrated off-ramp signal control (IOSC) model

This section presents the integrated off-ramp signal control (IOSC) model, consisting of the OQI module in the previous section and the signal design module (Chen and Chang, 2013), and its performance comparison with TRANSYT-7F under various experimental traffic scenarios. The necessity of accounting for the potential off-ramp queue spillback under different volume levels at an interchange will also be discussed.

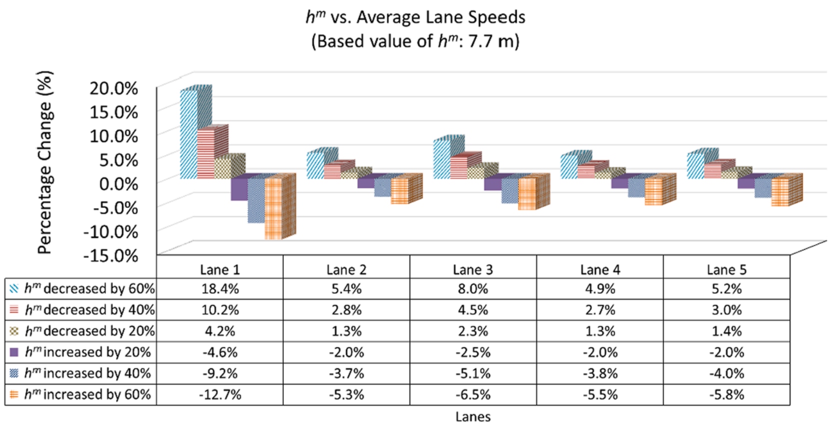

	Lane 1	Lane 2	Lane 3	Lane 4	Lane 5
h^m decreased by 60%	18.4%	5.4%	8.0%	4.9%	5.2%
h^m decreased by 40%	10.2%	2.8%	4.5%	2.7%	3.0%
h^m decreased by 20%	4.2%	1.3%	2.3%	1.3%	1.4%
h^m increased by 20%	-4.6%	-2.0%	-2.5%	-2.0%	-2.0%
h^m increased by 40%	-9.2%	-3.7%	-5.1%	-3.8%	-4.0%
h^m increased by 60%	-12.7%	-5.3%	-6.5%	-5.5%	-5.8%

Fig. 19. Relative changes in the average lane speed with respect to h^m.

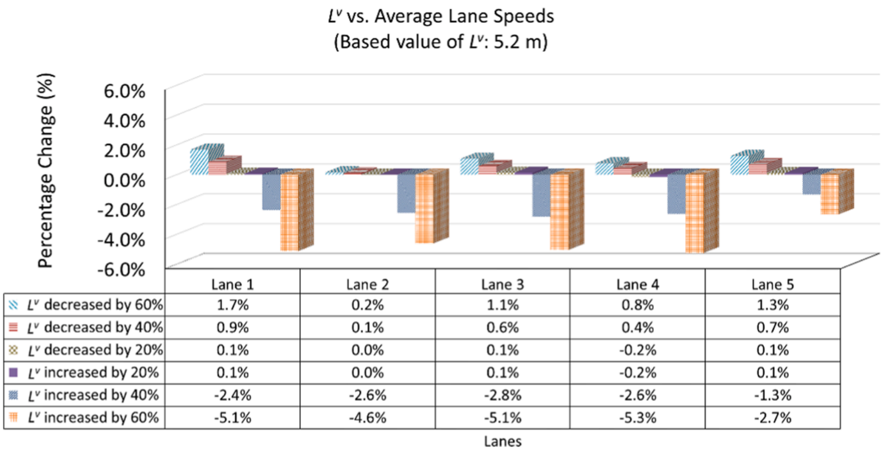

	Lane 1	Lane 2	Lane 3	Lane 4	Lane 5
L^v decreased by 60%	1.7%	0.2%	1.1%	0.8%	1.3%
L^v decreased by 40%	0.9%	0.1%	0.6%	0.4%	0.7%
L^v decreased by 20%	0.1%	0.0%	0.1%	-0.2%	0.1%
L^v increased by 20%	0.1%	0.0%	0.1%	-0.2%	0.1%
L^v increased by 40%	-2.4%	-2.6%	-2.8%	-2.6%	-1.3%
L^v increased by 60%	-5.1%	-4.6%	-5.1%	-5.3%	-2.7%

Fig. 20. Relative changes in the average lane speed with respect to L^v.

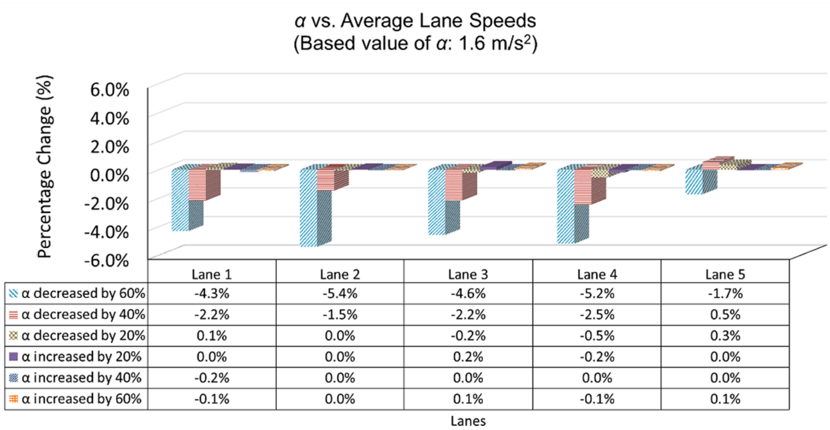

	Lane 1	Lane 2	Lane 3	Lane 4	Lane 5
α decreased by 60%	-4.3%	-5.4%	-4.6%	-5.2%	-1.7%
α decreased by 40%	-2.2%	-1.5%	-2.2%	-2.5%	0.5%
α decreased by 20%	0.1%	0.0%	-0.2%	-0.5%	0.3%
α increased by 20%	0.0%	0.0%	0.2%	-0.2%	0.0%
α increased by 40%	-0.2%	0.0%	0.0%	0.0%	0.0%
α increased by 60%	-0.1%	0.0%	0.1%	-0.1%	0.1%

Fig. 21. Relative changes in the average lane speed with respect to α.

3.1. The intersection signal design module

Note that each intersection approach, as shown in Fig. 22, in the control boundary is divided into the following sub-segments to reflect the evolution of congested traffic flows along each intersection approach, where

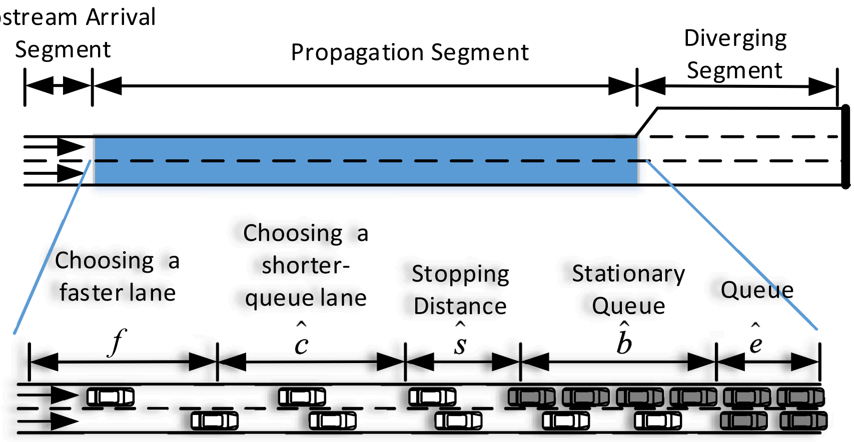

Fig. 22. Link decomposition of the intersection signal design module.

- $\widehat{e}$ sub-segment: the length of the shorter queue between two through lanes;
- $\widehat{b}$ sub-segment: the difference between two queue lengths in two through lanes;
- $\widehat{s}$ sub-segment: the stopping distance for vehicles evolving from moving to the standing queue status;
- $\widehat{c}$ sub-segment: the travel distance for drivers from perceiving the intersection queue to join the moving queue; and
- $\widehat{f}$ sub-segment: the travel distance within which drivers from the upstream link have not yet been affected by the intersection's queue condition.

Table 5 shows the notations used in the intersection signal design module.

For each intersection approach, the following equations are proposed to describe its traffic evolution. A more detailed description of the intersection signal design module can be found elsewhere (Chen and Chang, 2013).

$$q_j^{\epsilon}(k) = \min\left\{\Phi_j(k), \widehat{S}_j^U(k)\right\} \tag{19}$$

$$\widehat{S}_j^U(k) = O_j^{\widehat{P}} - N_j^{\widehat{P}}(k) - W_j^{\widehat{P}}(k) \tag{20}$$

$$\widehat{n}_{j,l}^{\vartheta,\Gamma}(k) = \min\left\{\widehat{u}_{j,l}^{\vartheta,\Gamma}(k), \widehat{S}_l^{\vartheta,\Gamma}(k)\right\}, \quad \text{for sub} - \text{segments } \widehat{b}, \widehat{c}, \text{ and } \widehat{f} \tag{21}$$

$$\widehat{u}_{j,l}^{\vartheta,\Gamma}(k) = \begin{cases} \widehat{N}_j^{\vartheta}(k) \cdot R_j^{\vartheta,\Gamma}(k) & \textit{for right} - \textit{ and left} - \textit{turning vehicles in sub} - \textit{segments } \widehat{b}, \widehat{c}, \textit{ and } \widehat{f} \\ \widehat{N}_j^{\vartheta}(k) \cdot R_j^{\vartheta,\Gamma}(k) \cdot I_{j,l}^{\vartheta}(k) & \textit{for through vehicles in sub} - \textit{segments } \widehat{b}, \widehat{c}, \textit{ and } \widehat{f} \end{cases} \tag{22}$$

$$\widehat{S}_l^{\vartheta,\Gamma}(k) = \begin{cases} \left(\widehat{O}_l^{\vartheta}(k) - \widehat{N}_l^{\vartheta}(k)\right) & \textit{for right} - \textit{ and left} - \textit{turning vehicles in sub} - \textit{segment } \widehat{b}, \widehat{c}, \textit{ or } \widehat{f} \\ \left(\widehat{O}_l^{\vartheta}(k) - \widehat{N}_l^{\vartheta}(k)\right) - \sum_{\widehat{\Gamma}=\text{left/rightturn}} \widehat{n}_{j,l}^{\vartheta,\widehat{\Gamma}}(k) & \textit{for through vehicles in sub} - \textit{segment } \widehat{b}, \widehat{c}, \textit{ or } \widehat{f} \end{cases} \tag{23}$$

$$Y_j(k) = \min\left\{\ddot{N}_j^{\widehat{P}}(k) + W_j^{\widehat{P}}(k), \rho_j^{\widehat{P}*}(k) \cdot v_j^{\widehat{P}}(k) \cdot \Delta t \Big/ 3600, O_{\widehat{j}}^{\widehat{D}} - N_{\widehat{j}}^{\widehat{D}}(k) - W_{\widehat{j}}^{\widehat{D}}(k)\right\}, \quad \widehat{j} \text{ is the receiving lane of the diverging segment} \tag{24}$$

$$\widehat{Y}_j(k) = \min\left\{N_j^{\widehat{D}}(k) + W_j^{\widehat{D}}(k), Q\,\widehat{G}_j(k)\Delta t \Big/ 3600, \sum_{j\in A} \widehat{S}_{\bar{j}}^U(k)\right\}, \quad A \in \text{the set of receiving lanes in the downstream link.} \tag{25}$$

Table 5
List of key variables used in the intersection signal design module.

C	Cycle length (sec)
C^{min}	Minimum cycle length (sec)
C^{Max}	Maximum cycle length (sec)
G_τ	Green time of phase τ (sec)
G^{min}	Minimum green time (sec)
$\widehat{G}_j(k)$	Green phase indicator of lane j at time interval k
$I^{\vartheta}_{j,l}(k)$	Lane-changing indicator of through vehicles in sub-segment ϑ. For sub-segments $\widehat{b}$ and $\widehat{c}$, $I^{\vartheta}_{j,l}(k) = 1$, if queue in lane l is shorter than it in lane j at time interval k; and $I^{\vartheta}_{j,l}(k) = 0$, otherwise. For sub-segment $\widehat{f}$, $I^{\vartheta}_{j,l}(k) = 1$, if speed of lane l is faster than it of lane j at time interval k; and $I^{\vartheta}_{j,l}(k) = 0$, otherwise.
$\widehat{I}_\tau$	Inter-green time of phase τ (sec)
$N^{\vartheta}_j(k)$	Number of vehicles of lane j in sub-segment ϑ at time interval k
$N_j^{\widehat{P}}(k)/N_j^{\widehat{D}}(k)$	Number of moving vehicles in lane j of the ***propagation/diverging segment*** at time interval k
$\widehat{N}^{\vartheta}_l(k)$	Number of moving vehicles in lane l of ***sub-segment*** ϑ at time interval k
$\ddot{N}_j^{\widehat{P}}(k)$	Number of moving vehicles in lane j of the ***propagation segment*** which can reach the downstream point of the propagation segment at time interval k
$\widehat{n}^{\vartheta,\Gamma}_{j,l}(k)$	Number of vehicles of turning movement Γ successful changing lane from lanes j to l in sub-segment ϑ of the propagation segment at time interval k
$O_j^{\widehat{P}}/O_j^{\widehat{D}}$	Total storage space in lane j of the ***propagation/diverging segment*** (vehicle)
$\widehat{O}^{\vartheta}_l(k)$	Total storage space in lane l of ***sub-segment*** ϑ at time interval k (vehicle)
Q	Discharging rate (vph)
$q^{\in}_j(k)$	Inflow rate of lane j at time interval k (vehicle per time interval)
$R^{\vartheta,\Gamma}_j(k)$	Turning ratio of vehicles of turning movement Γ in lane j of sub-segment ϑ at time interval k
$\widehat{S}^{U}_j(k)$	Remaining space of lane j in the ***upstream arrival segment*** at time interval k (vehicle)
$\widehat{S}^{\vartheta,\Gamma}_l(k)$	Remaining space of lane l in sub-segment ϑ for vehicles of turning movement Γ at time interval k (vehicle)
Δt	Time interval duration (sec)
$\widehat{u}^{\vartheta,\Gamma}_{j,l}(k)$	Number of vehicles of turning movement Γ intending to change from lanes j to l in sub-segment ϑ at step time interval k
$v_j^{\widehat{P}}(k)$	Average speed of lane j of the propagation segment at time interval k (kph)
$W_j^{\widehat{P}}(k)/W_j^{\widehat{D}}(k)$	Number of queuing vehicles in lane j of the ***propagation/diverging segment*** at time interval k
$Y_j(k)$	Number of vehicles in lane j of the ***propagation segment*** to the receiving lane of the ***diverging segment*** at time interval k
$\widehat{Y}_j(k)$	Number of vehicles discharging from lane j of diverging segment at time interval k
$\rho_j^{\widehat{P}*}(k)$	Density of lane j of the propagation segment at time interval k (after accommodating lane-changing vehicles) (veh/km)
$\Phi_j(k)$	Demand of lane j at time interval k (vehicle per time interval)

$$C \geq C^{min} \tag{26}$$

$$C \leq C^{Max} \tag{27}$$

$$G_\tau \geq G^{min} \tag{28}$$

$$\sum_{\tau} (G_\tau + \widehat{I}_\tau) = C \tag{29}$$

3.2. The objective functions and constraints

For near-saturated, saturated, or over-saturated traffic condition, one may choose the objective function of maximizing the total throughput, as shown in Eq. (30) for the proposed control. In contrast, for under-saturated traffic condition, minimizing the total travel time by all vehicles in the control area, as shown in Eq. (31), shall be selected as the control objective.

$$Max \sum_{k=1}^{K} \sum_{j=\Psi^{out}} q_j(k) \tag{30}$$

$$min \sum_{k=1}^{K} \left(\sum_{j \in \Pi} \widehat{N}_j(k) + \sum_{\varphi \in \Lambda} W_\varphi(k) \right) \bullet \Delta t \tag{31}$$

where, Ψ^{out} is the set of outgoing boundary lanes; K is the number of total time intervals; $\widehat{N}_j(k)$ is the number of vehicles in lane j at time interval k; W_φ is the number of vehicles waiting at demand entry node φ at time interval k; Π and Λ are the sets of lanes and demand entry nodes, respectively.

All constraints for the entire IOSC model include:
Freeway mainline related constraints: Eqs. (1), (2), (4)–(17)
Arterial related constraints (for every approach of intersections): Eqs. (19)–(25)
Signal timing related constraints: Eqs. (26)–(29)

3.3. Solution algorithm

This study employs the genetic algorithm by Liu and Chang (2011) to identify the set of optimal decision variables. Working within the interaction environment shown in Fig. 1, the core of the solution algorithm comprises the following key steps:
Step-1: Generate a *population set* randomly.
Step-2: For each *individual* in the *population set*
Step-2.1: Decode it to a signal timing plan based on the scheme proposed by Liu and Chang (2011).
Step-2.2: Determine the value of the objective function according to the signal timing plan.
Step-2.3: Evaluate corresponding fitness with the objective function value.
Step-3: Process the crossover and mutation procedure based on the fitness evaluation.
Step-4: Generate a new *population set*.
Step-5: Repeat *steps 2* to *4* until a stop criterion is satisfied.
Step-6: Output the optimal cycle length and splits.

3.4. Application for design of an off-ramp signal

Fig. 23 shows the control area for the case study site in Taiwan, designed to demonstrate the necessity of accounting for the impacts of ramp queues on the freeway segment in design of the local off-ramp signal. Both the key geometric features and existing intersection turning ratios, along with phase sequence, are further illustrated in Fig. 24. Different from the state of the practice, the target area for the off-ramp signal design comprises not only all intersection legs, but also the freeway segment likely affected by queue length developed on its off-ramp leg. Hence, the control objective for the signal is thus to minimize the total delay or to maximize throughput for the entire control area, including both the freeway and all intersection approaches, based on the OQI module developed in this study.

Conceivably, the necessity of accounting for off-ramp queue impacts in the signal design varies with not only the distribution of intersection volumes among all approaches, but also the flow rates on the off-ramp and the freeway mainline segment. Hence, the case study is designed to show their interrelations with the following three scenarios summarized in Table 6:

- **Scenario 1**: high volumes on the freeway mainline, the off-ramp, and the local arterial traffic.
- **Scenario 2**: same freeway and the off-ramp volumes as in Scenario 1 but low flow rates for all other intersection approaches.
- **Scenario 3**: low freeway and the off-ramp volumes but the same high flow rates as in Scenario 1 at all other intersection approaches.

Note that the control objective of maximizing the total system throughput has been chosen in this case study to generate the

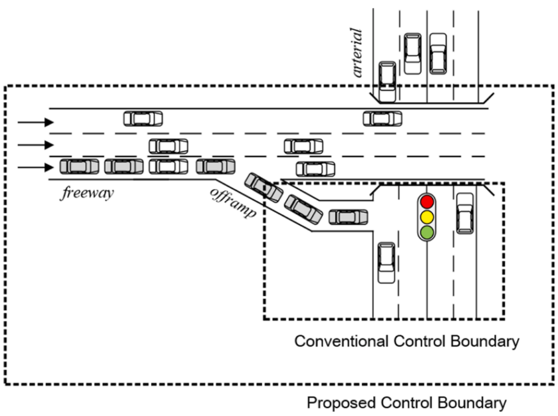

Fig. 23. Conventional and proposed control boundaries.

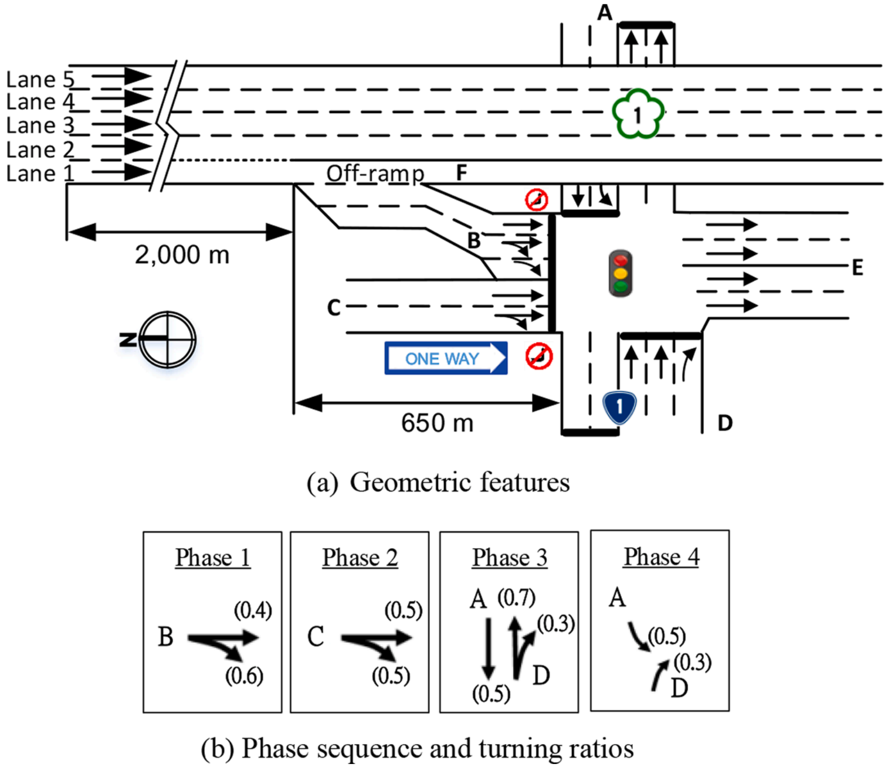

Fig. 24. Key features of the study site.

Table 6
List of experimental scenarios.

Scenarios	Volume distribution (in vph)				
	Freeway	A	B (off-ramp)	C	D
1	10,000	1,000	1,200	600	1,000
2	10,000	600	1,200	300	600
3	6,000	1,000	720	600	1,000

Table 7
Key model parameters of the signal design module and genetic algorithm.

Parameter	Value
Flow Model for Surface Street	
Free-flow speed for surface streets	50 kph
Jam density[a]	130 veh/km/lane
Saturation flow rate for surface streets[a]	1,600 vphpl
Signal Parameters	
Max cycle length	150 s
Minimal green time	15 s
Inter-green time	3 s
Genetic Algorithm[b]	
Population size	30
Maximum number of generations	200
Mutation rate	0.03
Crossover probability	0.5

Notes: [a]Values from Chen and Chang (2013); and [b]values from Liu and Chang (2011).

optimized cycle length and splits of the traffic signals with GA. Table 7 shows the list of key model parameters used in search of the optimal solution. The free flow speed of the surface streets is set to 50 kph, which is 10 kph higher than the speed limit, conforming the tolerance range of police enforcement for speeding vehicles at the case study site. Jam density and saturation flowrate are based on the results from the previous research (Chen and Chang, 2013). Signal constraints, including the maximum cycle, minimum green, and inter-green time are preset parameters. The resulting MOEs, including delay and throughput, under the optimized signal plan for performance comparison are from the simulation outputs of TSIS 6.3, a stochastic microsimulation software by FHWA (McTrans, 2011).

Note that, none of the existing studies in the literature on the off-ramp signal design has addressed the same concerns raised in this study, and employed the control objective of maximizing the total benefit of the freeway and arterial users within the control area. Therefore, for performance comparison, this study has compared the proposed model with the state-of-the-art signal optimization tool, TRANSYT-7F, which allows the users to set the disutility index (DI) for over-length queues (i.e., the queuing penalty) at selected approaches. For a fair comparison, the off-ramp was modeled as an intersection approach in the TRANSYT-7F and the queuing penalty was chosen as the DI.

Comparison results with respect to the cycle length and green splits produced with the proposed IOSC model and TRANSYT-7F are summarized in Table 8. Noticeably, under Scenario-1 of congested traffic conditions and high off-ramp volume, incorporating the queue spillback impacts in the design for the IOSC model yields the cycle length of 115 s and the green split of 0.4 for the off-ramp approach, much higher than the split of 0.22 for the same intersection approach under the comparable cycle length of 120 s by TRANSYT-7F.

By reallocating a longer green duration to accommodate the high off-ramp volume, the signal plan with the IOSC model can achieve about a 9% (see Table 9) increase in the total system throughput, mostly on the freeway segment (from 6,681 vph to 8,087 vph) due to the prevention of queue spillback from the off-ramp flows (see Fig. 25(a)). The benefits of minimizing the off-ramp queue impacts are also reflected on the 56% reduction in the total system delay (see Table 9), attributing mainly to the decrease in total vehicle delay, from 15,160 to 720 vehicle-minutes (Fig. 26(a)) on the freeway segment.

Note that such substantial improvements on the freeway in Scenario-1 are due to the allocation of a longer green time to the off-ramp flows, which will inevitably reduce the available green times for all other intersection approaches and thus increase their total delays. For instance, the conventional design practice with TRANSYT, neglecting the off-ramp queue impacts, tends to allocate more green times to phases 2 (0.21 vs. 0.13) and 3 (0.31 vs. 0.18) to discharge more non-off-ramp flows, and thus result in more throughput and less delays for those intersection approaches (see Fig. 25(a) and Fig. 26(a)).

However, since the off-ramp queue spillback, if taking place, may cause an exponential delay increase and throughput reduction on the freeway segment due to the non-linear nature of traffic flow dynamics, such a trade-off, reflecting the minimal impacts on the surface traffic delays, certainly deserves the implementation by the traffic agency responsible for contending with corridor traffic congestion.

Scenario-2 highlights the traffic conditions where the intersection receiving the off-ramp flows must accommodate only relatively low surface traffic volumes from all other approaches. Hence, both the IOSC model and the TRANSYT-7F are expected to be capable of allocating sufficient green duration to the off-ramp flows so that the traffic queues are less likely to spill back onto the freeway mainline. The results of green splits and MOEs shown in Table 8 and Table 9, respectively, clearly confirm such pre-assessment, where both models yield a quite similar set of green splits, and the shorter cycle length produced by the IOSC model seems to contribute to the 16% delay reduction (see Table 9) for the entire control area. Further comparisons with respect to the delay by intersection approach are also evidence that off-ramp vehicles (Fig. 26(b)) experience the most delay reduction under the IOSC model's signal plan. Note that all intersection approaches and the freeway segment have nearly the same throughputs under both models, due mainly to the distribution of low arterial volumes that produce no-residual queues per cycle and no off-ramp queues during the control period.

Scenario-3 is designed to evaluate the IOSC model's sensitivity, as it should view the off-ramp intersection as a typical local intersection if the freeway volume is relatively light and the off-ramp queue is of no concern to the traffic control operations. As such, both models are expected to yield approximately the same level of MOEs at either the entire system level or by intersection approach. The simulation results, shown in Table 9, Fig. 25(c) and Fig. 26(c), indeed are consistent with the expectation that both models perform indifferently under a standard statistical test in this traffic scenario, regardless of the selected MOE.

Table 8
Optimal signal plans.

Scenario	Model	Cycle length (sec)	Green split			
			Phase 1	Phase 2	Phase 3	Phase 4
1	IOSC Model	115	0.40	0.13	0.18	0.18
	TRANSYT-7F	120	0.22	0.21	0.31	0.17
2	IOSC Model	103	0.36	0.15	0.19	0.18
	TRANSYT-7F	126	0.34	0.14	0.22	0.20
3	IOSC Model	95	0.16	0.20	0.32	0.20
	TRANSYT-7F	84	0.19	0.21	0.24	0.21

Table 9
MOEs.

Scenario	Delay (veh-min)			Throughput (vph)		
	TRANSYT-7F	IOSC Model	Percent Change[1]	TRANSYT-7F	IOSC Model	Percent Change[1]
1	25,583	11,200	−56.2%	10,715	11,680	9.0%
2	2,823	2,369	−16.1%	10,809	10,755	−0.5%
3	5,575	5,530	−0.8%	8,153	8,325	2.1%

[1] Percent Change $= [(MOE_{IOSC\ model} - MOE_{TRANSYT\text{-}7F})/MOE_{TRANSYT\text{-}7F}] \cdot 100\%$.

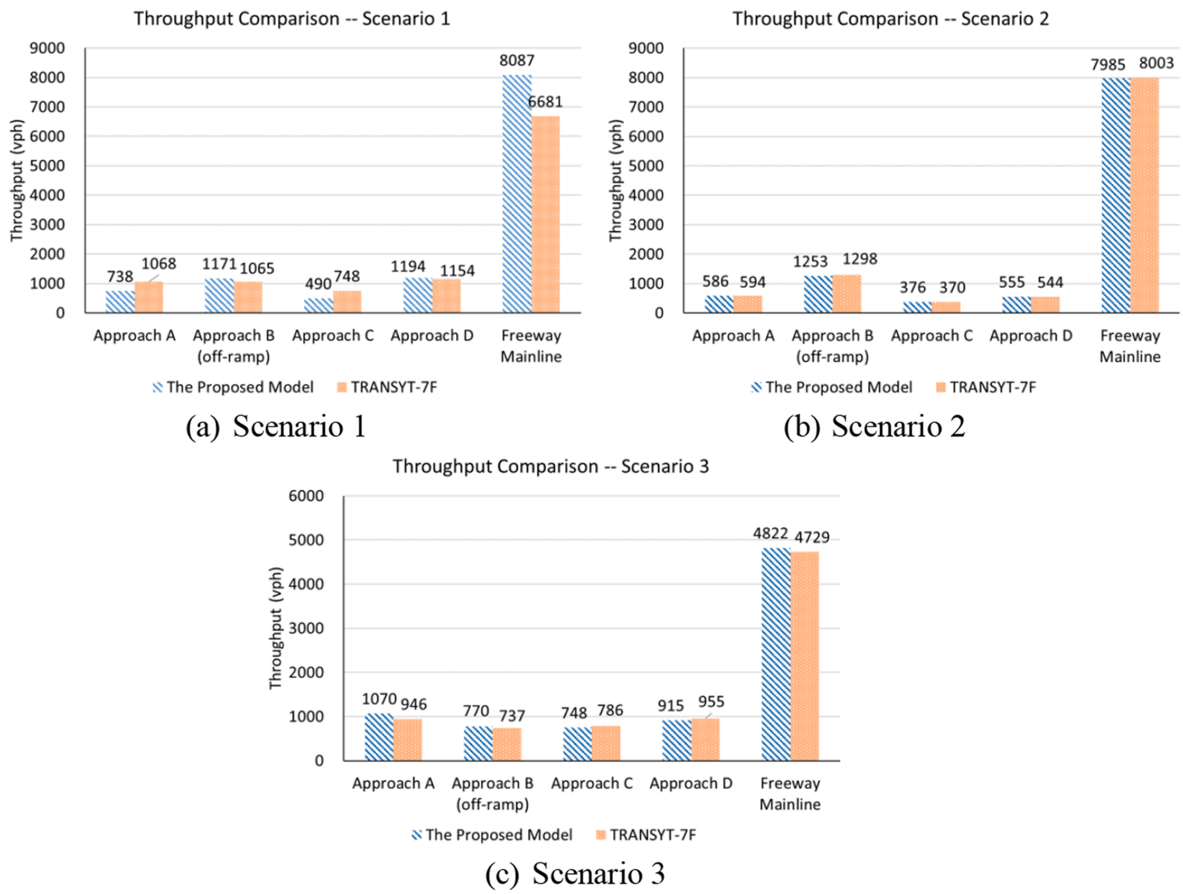

Fig. 25. Throughputs of scenarios.

4. Conclusions

This paper has presented an integrated off-ramp signal control model to tackle the off-ramp queue spillback issue, that is, one of the main contributors to the formation of freeway bottlenecks, especially during congested commuting periods. The results from both field data comparison and extensive numerical analyses have yielded the following imperative findings. First, failing to account for off-ramp queue impacts on the freeway in design of the off-ramp signal will often allocate insufficient green time for the intersection approach designated to accommodating the freeway exiting flows, and consequently cause congested and chaotic traffic conditions on the freeway due to the spillover effects of excessive off-ramp queue. Secondly, to mitigate the congestion due to a local bottleneck in the vicinity of an interchange, the signal control objective for the off-ramp intersection shall be to maximize the total throughput (or minimize the total delay) for the control zone that includes both the freeway and arterial segments.

Most importantly, the field evaluation results conducted in this study confirm that the complex impacts of off-ramp queue spillover on the freeway's traffic conditions, manifested through the extensive mandatory and discretionary lane changes, can be reliably captured with rigorously formulated mesoscopic relations. By incorporating such relations in the signal optimization process, the proposed model under extensive numerical analyses and simulation evaluation has demonstrated its effectiveness in maximizing the benefits to both the off-ramp intersection and the connected freeway segment. Such benefits are especially significant if the off-ramp

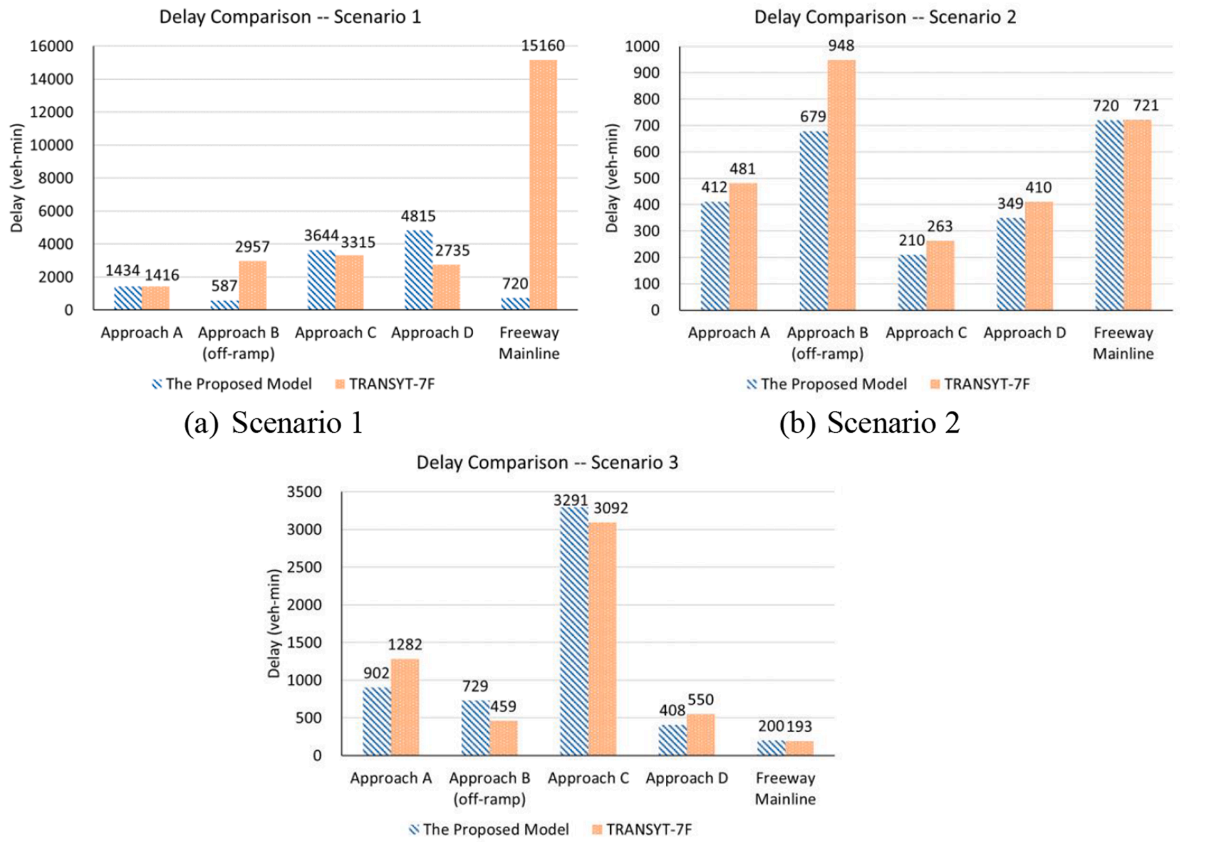

(a) Scenario 1

(b) Scenario 2

(c) Scenario 3

Fig. 26. Delays of scenarios.

intersection is on a congested arterial and needs to accommodate a large volume of exiting freeway flows.

Future studies along this line will include an extension of the proposed off-ramp control model to its neighboring signals responsible for feeding traffic flows to the on-ramps in the same interchange. Further integration of both on-ramp and off-ramp controls in the same interchange to alleviate a freeway's local bottlenecks will also be an essential task. In addition, to ensure an efficient progression of traffic flows on the arterial for accommodating large volume of both on-ramp and off-ramp flows, the design of a multi-path signal progression system that can offer a progression band for not only the through traffic but also vehicle streams heading to different destinations will be a challenging and imperative on-going work. Furthermore, to facilitate the applications of the proposed model on different highway segments, the development of an automated model calibration system with field data is one of our on-going research tasks.

Table A1
Estimated parameter from calibrations.

Parameters	**Initial**[a]		**Final**[b]	
	Estimation	t-value	Estimation	t-value
β_1	0.184	13.8 (***)	0.191	16.2 (***)
β_2	0.0947	6.1 (***)	0.102	7.6 (***)
β_3	0.455	10.9 (***)	0.456	12.5 (***)
β_4	−2.221	−20.4 (***)	−2.197	−23.6 (***)
	Adjusted R^2: 0.839 F-statistic: 1081 on 4 and 825 DF p-value: <2.2e-16		Adjusted R^2: 0.832 F-statistic: 1456 on 4 and 1173 DF, p-value: <2.2e-16	

Note: Signif. codes: ***: <0.001; **:0.001; *:0.05.
[a] 70% of data in NGSIM are used.
[b] 100% data in NGSIM are used.

CRediT authorship contribution statement

Yen-Yu Chen: Conceptualization, Methodology, Software, Validation, Formal analysis, Investigation, Data curation, Visualization, Writing - original draft. **Yen-Hsiang Chen:** Methodology, Validation, Formal analysis, Data curation, Writing - original draft. **Gang-Len Chang:** Conceptualization, Supervision, Writing - review & editing.

Declaration of Competing Interest

The authors declare that they have no known competing financial interests or personal relationships that could have appeared to influence the work reported in this paper.

Appendix A

Calibration and Validation of the Discretionary Lane Change (DLC) Function

Step 1- Initial calibration: Ground truth data extracted from NGSIM are separated into two sets: 70% for initial calibration and 30% for validation. The regression results from this step are summarized in Table A1.

Step 2- Model performance evaluation: The performance of the model is evaluated by comparing the predicted and actual lane-changing fractions of through vehicles and the numbers of lane changes with RMSE and MAE on a 1,275 ft. stretch:

Lane-changing fraction per minute: RMSE = 0.160; MAE = 0.0794

Number of lane changes per minute: RMSE = 1.81; MAE = 1.17

Step 3- Parameter finalization: Given the acceptable performance results, the initial set of parameters is then updated with the full set of data to enhance their stability.

References

Cassidy, M.J., Anani, S.B., Haigwood, J.M., 2002. Study of freeway traffic near an off-ramp. Transport. Res. A: Pol. 36 (6), 563–572. https://doi.org/10.1016/S0965-8564 (01)00016-7.

Chang, G.L., Kao, Y.M., 1991. An empirical investigation of macroscopic lane-changing characteristics on uncongested multilane freeways. Transport. Res. A: Gen. 25 (6), 375–389. https://doi.org/10.1016/0191-2607(91)90015-I.

Chen, Y.Y., Chang, G.L., 2013. A macroscopic signal optimization model for arterials under heavy mixed traffic flows. IEEE Trans. Intell. Transp. Syst. 15 (2), 805–817. https://doi.org/10.1109/TITS.2013.2289961.

Daganzo, C.F., 1997. A continuum theory of traffic dynamics for freeways with special lanes. Transport. Res. B: Meth. 31 (2), 83–102. https://doi.org/10.1016/S0191-2615(96) 00017-3.

Daganzo, C.F., Cassidy, M.J., Bertini, R.L., 1999. Possible explanations of phase transitions in highway traffic. Transport. Res. A: Pol. 33 (5), 365–379. https://doi.org/10.1016/S0965-8564(98)00034-2.

[dataset] Federal Highway Administration (FHWA), 2016. NGSIM Program US Route 101 data, https://ops.fhwa.dot.gov/trafficanalysistools/ngsim.htm.

Gazis, D.C., Herman, R., Weiss, G.H., 1962. Density oscillations between lanes of a multilane highway. Oper. Res. 10 (5), 658–667. https://doi.org/10.1287/opre.10.5.658.

Gipps, P.G., 1986. A model for the structure of lane-changing decisions. Transport. Res. B: Meth. 20 (5), 403–414. https://doi.org/10.1016/0191-2615(86)90012-3.

Highway Capacity Manual, 2016. A guide for multimodal mobility analysis, 6th edition. Transportation Research Board, Washington, D.C.

Jin, W.L., 2010. Macroscopic characteristics of lane-changing traffic. Transport. Res. Rec. 2188 (1), 55–63. https://doi.org/10.3141/2188-07.

Kerner, B.S., Rehborn, H., 1997. Experimental properties of phase transitions in traffic flow. Phys. Rev. Lett. 79 (20), 4030–4033. https://doi.org/10.1103/PhysRevLett.79.4030.

Koutsoyiannis, A., 1973. Theory of Econometrics: An introductory exposition of econometric methods. McMillan Press, London.

Laval, J.A., Daganzo, C.F., 2006. Lane-changing in traffic streams. Transport. Res. B: Meth. 40 (3), 251–264. https://doi.org/10.1016/j.trb.2005.04.003.

Li, Z., Chang, G.L., Natarajan, S., 2009. An integrated off-ramp control model for freeway traffic management. Presented at 15th World Congress on Intelligent Transportation Systems, New York.

Lim, K., Kim, J.H., Shin, E., Kim, D.G., 2011. A signal control model integrating arterial intersections and freeway off-ramps. KSCE J. Civ. Eng. 15 (2), 385–394. https://doi.org/10.1007/s12205-011-0880-y.

Liu, H.X., Wu, X., Michalopoulos, P.G., 2007. Improving queue size estimation for Minnesota's stratified zone metering strategy. Transport. Res. Rec. 2012 (1), 38–46. https://doi.org/10.3141/2012-05.

Liu, Y., Chang, G.L., 2011. An arterial signal optimization model for intersections experiencing queue spillback and lane blockage. Transport. Res. C: Emer. 19 (1), 130–144. https://doi.org/10.1016/j.trc.2010.04.005.

Liu, Y., Chang, G.L., Yu, J., 2011. An integrated control model for freeway corridor under nonrecurrent congestion. IEEE Trans. Veh. Technol. 60 (4), 1404–1418. https://doi.org/10.1109/TVT.2011.2115264.

Munjal, P.K., Pipes, L.A., 1971. Propagation of on-ramp density perturbations on unidirectional two-and three-lane freeways. Transport. Res. 5 (4), 241–255. https://doi.org/10.1016/0041-1647(71)90036-0.

Muñoz, J.C., Daganzo, C.F., 2002. The bottleneck mechanism of a freeway diverge. Transport. Res. A: Pol. 36 (6), 483–505. https://doi.org/10.1016/S0965-8564(01)00017-9.

Newell, G.F., 1999. Delays caused by a queue at a freeway exit ramp. Transport. Res. B: Meth. 33 (5), 337–350. https://doi.org/10.1016/S0191-2615(98)00039-3.

Oliver, R.M., Lam, T., 1965. Statistical experiments with a two-lane flow model, No. ORC-65-20. California University Berkeley Operations Research Center.

Pahl, J., 1972. Lane-change frequencies in freeway traffic flow. Highway Res. Rec. 409, 17–33.

Rudjanakanoknad, J., 2012. Capacity change mechanism of a diverge bottleneck. Transport. Res. Rec. 2278 (1), 21–30. https://doi.org/10.3141/2278 -03.

Spiliopoulou, A., Kontorinaki, M., Papageorgiou, M., Kopelias, P., 2014a. Macroscopic traffic flow model validation at congested freeway off-ramp areas. Transport. Res. C: Emer. 41, 18–29. https://doi.org/10.1016/j.trc.2014.01.009.

Spiliopoulou, A., Kontorinaki, M., Papamichail, I., and Papageorgiou, M., 2013. Real-time route diversion control at congested motorway off-ramp areas-Part I: User-optimum route guidance. In Proceeding of 16th International IEEE Conference on Intelligent Transportation Systems (ITSC 2013), 2119-2125. DOI: 10.1109/ITSC.2013.67 28542.

Spiliopoulou, A., Kontorinaki, M., Papamichail, I., Papageorgiou, M., 2014b. Real-time route diversion control at congested off-ramp areas-Part II: route guidance versus off-ramp closure. Procedia Soc. Behav. Sci. 111 (5), 1102–1111. https://doi.org/10.1016/j.sbspro. 2014.01.145.
Spiliopoulou, A., Kontorinaki, M., Papamichail, I., Papageorgiou, M., 2018. Real-time route diversion control at congested freeway off-ramp areas. Transport. Res. A: Pol. 107, 90–105. https://doi.org/10.1016/j.tra.2017.11.017.
Spiliopoulou, A., Papageorgiou, M., Herrera, J.C., Muñoz, J.C., 2016. Real-time merging traffic control at congested freeway off-ramp areas. Transport. Res. Rec. 2554 (1), 101–110. https://doi.org/10.3141/2554-11.
Sun, J., Ma, Z., Chen, X., 2017. Some observed features of traffic flow phase transition at urban expressway diverge bottlenecks. Transportmetrica B 6 (4), 320–331. https://doi.org/10.1080/21680566.2017.1336127.
Toledo, T., Koutsopoulos, H.N., Ben-Akiva, M., 2007. Integrated driving behavior modeling. Transport. Res. C: Emer. 15 (2), 96–112. https://doi.org/10.1016/j. trc.2007.02. 002.
TSIS Users Guide, 2011. McTrans. University of Florida, Gainesville, FL.
Wiedemann, Reiter, Reiter, U., 1992. Microscopic traffic simulation: the simulation system MISSION, background and actual state. Project ICARUS (V1052) Final Report 2, 1–53.
Yang, Q., Koutsopoulos, H.N., 1996. A microscopic traffic simulator for evaluation of dynamic traffic management systems. Transport. Res. C: Emer. 4 (3), 113–129. https://doi.org/10.1016/S0968-090X(96)00006-X.
Yang, X., Cheng, Y., Chang, G.L., 2018. Integration of adaptive signal control and freeway off-ramp priority control for commuting corridors. Transport. Res. C: Emer. 86, 328–345. https://doi.org/10.1016/j.trc.2017.11.019.
Yang, X., Lu, Y., Chang, G.L., 2014. Dynamic signal priority control strategy to mitigate off-ramp queue spillback to freeway mainline segment. Transport. Res. Rec. 2438 (1), 1–11. https://doi.org/10.3141/2438-01.
Zhao, J., Liu, Y., 2016. Integrated signal optimization and non-traditional lane assignment for urban freeway off-ramp congestion mitigation. Transport. Res. C: Emer. 73, 219–238. https://doi.org/10.1016/j.trc.2016.11.003.